# Outer membrane lipoprotein DolP interacts with the BAM complex and promotes fitness during envelope stress response

David Ranava[1,§], Yiying Yang[1,§], Luis Orenday-Tapia[1,§], François Rousset[2], Catherine Turlan[1], Lun Cui[2], Violette Morales[1], Cyril Moulin[1], Gladys Munoz[1], Jérôme Rech[1], Anne Caumont-Sarcos[1], Cécile Albenne[1], David Bikard[2], Raffaele Ieva[1*]

[1]Laboratoire de Microbiologie et Génétique Moléculaires (LMGM), Centre de Biologie Intégrative (CBI), Université de Toulouse, CNRS, UPS, Toulouse 31062, France.

[2]Synthetic Biology Group, Microbiology Department, Institut Pasteur, Paris 75015, France.

[§]These authors contributed equally to this paper.

*Correspondance to :

Raffaele Ieva, raffaele.ieva@univ-tlse3.fr

**Abstract**

In Gram-negative bacteria, coordinated remodelling of the outer membrane (OM) and the peptidoglycan is crucial for envelope integrity. Envelope stress caused by unfolded OM proteins (OMPs) activates sigmaE($\sigma^E$) in Enterobacteria. Whereas $\sigma^E$ upregulates biogenesis factors, including the $\beta$-barrel assembly machinery (BAM) that catalyzes OMP-folding, elevated $\sigma^E$ activity can be detrimental for OM integrity. We report that DolP (YraP), a $\sigma^E$-upregulated OM lipoprotein needed for envelope integrity, is a novel interactor of BAM and that BamA is a critical determinant of the BAM-DolP complex. Mid-cell recruitment of DolP had been reported to promote septal peptidoglycan remodelling during cell division, but the role of DolP during envelope stress was unknown. Using a synthetic-defect CRISPRi screen, we found that *dolP* is critical in cells with elevated or constitutive $\sigma^E$ activation. Differently from other $\sigma^E$-upregulated proteins, DolP is not directly implicated in OMP assembly. Envelope stress or OM-overaccumulating BamA, however, interferes with DolP septal recruitment. Taken together, our results uncover DolP as a fitness factor during $\sigma^E$ activation, and support a model where differential septal recruitment of DolP contributes to link envelope stress to a late step of cell division.

## Introduction

The outer membrane (OM) of Gram-negative bacteria forms a protective barrier against harmful compounds, including several antimicrobials. This envelope structure surrounds the inner membrane and the periplasm that contains the peptidoglycan, a net-like structure made of glycan chains and interconnecting peptides. During cell division, the multi-layered envelope structure is remodelled by the divisome machinery [1]. At a late step of division, septal peptidoglycan synthesized by the divisome undergoes splitting, initiating the formation of the new poles of adjacent daughter cells. Finally, remodelling of the OM barrier completes formation of the new poles in the cell offspring. The mechanisms by which cells coordinate OM remodelling with peptidoglycan splitting, preserving the permeability barrier of this protective membrane, are ill-defined [2].

Integral outer membrane proteins (OMPs) are crucial to maintain the OM permeability barrier. OMPs fold into amphipathic β-barrel structures that span the OM and carry out a variety of tasks. Porins are OMPs that facilitate the diffusion of small metabolites. Other OMPs function as cofactor transporters, secretory channels, or machineries for the assembly of proteins and lipopolysaccharide (LPS) [3,4], a structural component of the external OM leaflet that prevents the diffusion of noxious chemicals [4]. The β-barrel assembly machinery (BAM) is a multi-subunit complex that mediates the folding and membrane insertion of OMPs transiting through the periplasm [5,6]. The essential and evolutionarily conserved BamA insertase subunit is an OMP consisting of an amino (N)-terminal periplasmic domain made of polypeptide transport-associated (POTRA or P) motifs and a carboxy (C)-terminal 16-stranded β-barrel membrane domain that catalyzes OMP biogenesis [7,8]. The flexible pairing of β-strands 1 and 16 of the BamA β-barrel controls a lateral gate connecting the interior of the barrel towards the surrounding lipid bilayer [9-12]. Conformational dynamics of the BamA β-barrel region proximal to the lateral gate is

69 thought to locally increase the entropy of the surrounding lipid bilayer [9,13,14] and
70 assist the insertion of nascent OMPs into the OM [11,15,16]. The N-terminal periplasmic
71 portion of BamA from the enterobacterium *Escherichia coli* contains five POTRA
72 motifs that serve as a scaffold for four lipoproteins, BamBCDE, which assist BamA
73 during OMP biogenesis [17-19]. The N-terminal POTRA motif is also the docking site of
74 the periplasmic chaperone SurA [20]. Together with the chaperones Skp and DegP,
75 SurA contributes to monitor unfolded OMPs transported into the periplasm by the
76 inner membrane general secretory (Sec) pathway [21,22].

77 Defective OMP assembly causes periplasmic accumulation of unfolded
78 protein transport intermediates. This envelope stress is signalled across the inner
79 membrane to induce a sigmaE ($\sigma^E$)-mediated transcriptional response [23]. In the
80 absence of stress, $\sigma^E$ is sequestered by the inner membrane-spanning RseA factor.
81 By-products of misfolded OMP turnover activate degradation of RseA, liberating $\sigma^E$
82 [24]. The $\sigma^E$ response copes with stress i) by upregulating genes involved in OMP
83 biogenesis, such as the *bam* genes [25], and ii) by lowering the OMP biogenesis
84 burden via a post-transcriptional mechanism [26]. Whereas $\sigma^E$ is essential [27], a tight
85 control of cytosolic $\sigma^E$ availability is necessary for optimal cell fitness and to prevent
86 a possible detrimental effect on the envelope [28-31]. Remarkably, the functions of a
87 number of genes upregulated by $\sigma^E$ remains unknown. Among those, *yraP* encodes
88 a ~20 kDa OM-anchored lipoprotein largely conserved in $\gamma$ and $\beta$ proteobacteria [32-
89 36]. YraP is crucial for OM integrity [34] and pathogenicity [32], and it was proposed to be
90 important for OMP biogenesis [34]. A recent study showed that YraP localizes at the
91 mid-cell during a late step of cell division, where it contributes to the regulation of
92 septal peptidoglycan splitting by an unknown mechanism [33]. These observations do
93 not explain why YraP is upregulated in response to $\sigma^E$ activation and how YraP
94 helps coping with envelope stress.

95 During cell division, envelope stress caused by defective OMP biogenesis
96 would place an additional burden on the already-complicated envelope reshaping

process faced by cells. It remains unknown whether stress caused by unfolded OMPs influences envelope remodelling at the forming poles of two adjacent daughter cells. Here we present a functional investigation of *yraP* prompted by a genome-wide synthetic-defect screen. We demonstrate genetic interactions of *yraP* with *bam* genes and we provide evidence that YraP can associate with the BAM complex via an interaction with the BamA subunit. YraP is not critical for OMP assembly but promotes fitness upon activation of the $\sigma^E$ response and under conditions that impair secretion or assembly of OMPs in the OM. Upon envelope stress or when BAM overaccumulates in the OM, YraP loses its association with the mid-cell, thus suggesting that YraP contributes to link envelope stress response and septal peptidoglycan hydrolysis during a late step of cell division. Hence, we propose to rename YraP as DolP (division- and OM stress-associated lipoprotein).

109 **Results**

110

111 **A genome-wide synthetic-defect screen identifies *dolP* genetic interactions**

112 The mutant allele Δ*dolP::kan* [37] was introduced into *E. coli* BW25113 by P1
113 transduction. The resulting Δ*dolP* strain grew normally on LB medium but was
114 highly susceptible to vancomycin, an antibiotic normally excluded from the OM of
115 wild-type (*dolP*$^+$) cells (Fig. 1A). The expression of C-terminally fused DolP variants
116 in place of the wild-type protein restored growth in the presence of vancomycin (Fig.
117 1A and Fig. S1B). This result supports the notion that DolP is important for envelope
118 integrity [33-36]. However, the role of DolP during envelope stress remains poorly
119 understood.

120 To gain insights into the function of DolP, we subjected Δ*dolP* cells to a
121 genome-wide synthetic-defect screen exploiting a Clustered Regularly Interspersed
122 Short Palindromic Repeat interference (CRISPRi) approach. Targeting of the
123 catalytically inactive dCas9 nuclease by gene-specific single guides RNAs
124 (sgRNAs) enables gene repression (Fig. 1B) [38]. The EcoWG1 sgRNA library
125 targeting the entire genome of *E. coli* MG1655 [39] was introduced into isogenic Δ*dolP*
126 or *dolP*$^+$ MG1655-derivative strains. The fitness of each knockdown was then
127 compared in these backgrounds by deep-sequencing of the sgRNA library after ~17
128 growth generations. The outputs obtained from two independent tests were highly
129 reproducible (Fig. S2A). A strong fitness defect in the Δ*dolP* strain was caused by
130 the targeting of *envC* (Fig. 1C, Fig. S2B and Tables S1 and S2), followed by the
131 targeting of *ftsX* and *ftsE* (Fig. 1C, Tables S1 and S2). A validation growth test
132 showed that the synthetic fitness defect observed for Δ*dolP* cells was caused by
133 dCas9-dependent silencing of *ftsX* and *envC* (Fig. 1D, panels 6 and 7). The ABC
134 transporter-like complex FtsE/FtsX has multiple roles in organizing the cell
135 divisome, including the recruitment of periplasmic EnvC, a LytM domain-containing
136 factor required for the activation of amidases that hydrolase septal peptidoglycan [40].

137 This peptidoglycan remodelling reaction is mediated by two sets of highly controlled
138 and partially redundant amidases, AmiA/AmiB and AmiC [41,42]. Whereas AmiA and
139 AmiB are activated at the inner membrane/peptidoglycan interface by the
140 coordinated action of FtsE/FtsX and EnvC, activation of AmiC requires the OM-
141 anchored LytM domain-containing lipoprotein NlpD [43,44]. Under laboratory
142 conditions, the activity of only one of these two pathways is sufficient for septal
143 peptidoglycan splitting, whereas inhibition of both pathways leads to formation of
144 chains of partially divided cells, *i.e.* cells that have begun to divide but are blocked
145 at the step of septal peptidoglycan splitting [44]. A recent report showed that *dolP* is
146 necessary to complete septal peptidoglycan splitting and to promote cell separation
147 when the AmiA/AmiB pathway is inactive, somehow linking DolP to AmiC activation
148 [33]. Thus, the reduced fitness caused by silencing of *envC, ftsE or ftsX* in Δ*dolP* cells
149 (Fig. 1C) may be explained by impaired cell separation when both the AmiA/AmiB
150 and the AmiC pathways are not active. In keeping with this notion, *amiA* itself was
151 found among the negative fitness hits of the CRISPRi screen (Fig. 1C). *amiB* was
152 not a hit (Table S1), probably because AmiA is sufficient to split septal
153 peptidoglycan in the absence of other amidases [45].

154 Most importantly, the CRISPRi approach identified novel *dolP*-genetic
155 interactions that had a score similar to that obtained for *amiA* (Fig. 1C). These
156 included an interaction with *rseA*, encoding the inner membrane $\sigma^E$-sequestering
157 factor, as well as with *bamD*, encoding an essential subunit of the BAM complex
158 [34,46]. In accordance with the screen output, a serial dilution assay confirmed that
159 silencing of *bamD* (as well as *bamE*, encoding a stoichiometric interactor of BamD)
160 impairs growth of cells lacking DolP (Fig. 1D, panels 8 and 9). In addition, the
161 interaction of *dolP* with *rseA* was also confirmed in the genetic background of the
162 BW25113 strain (Fig. 1E). Further genes, mainly involved in OMP biogenesis and
163 homeostasis, or more generally in protein secretion, had a lower interaction score
164 (Table S1 and Fig. S2C) and are highlighted in Fig. 1C. These include genes

165 encoding the Sec ancillary complex SecDF-YajC, which contributes to the efficient
166 secretion of proteins including OMPs [22] and was shown to interact with the BAM
167 complex [47,48]. Collectively, the results of the CRISPRi screen indicate that the
168 function of DolP is particularly critical for cell fitness upon inactivation of septal
169 peptidoglycan hydrolysis by AmiA, as well as when OMP biogenesis is impaired.

170

171 **DolP does not play a crucial role in OMP biogenesis but improves fitness**
172 **when the OM undergoes stress**

173 At a first glance, the newly identified genetic interaction between *dolP* and
174 *bamD* (Figs. 1C and 1D) points to a possible role of DolP in OMP biogenesis.
175 However, we found that the protein composition of the crude envelope fraction (Fig.
176 S3A) and more specifically the assembly of two trimeric porins, LamB and OmpC
177 (Figs. S3B and S3C) were not affected by the deletion of *dolP*. Similarly, the
178 assembly kinetics of an autotransporter OMP was not impaired in Δ*dolP* cells (Fig.
179 S3D). Importantly, cells lacking DolP had a normal $\sigma^E$ activity as the expression of
180 $\sigma^E$-regulated genes, such as *bamA* or *bamE*, was not upregulated (Fig. 2A). Taken
181 together, these observations suggest that DolP does not play a major function in
182 OMP biogenesis. Yet, DolP promotes optimal cell fitness under envelope stress
183 conditions. The genetic interaction of *dolP* with *bamD* or *surA* (Fig. 1C) may also
184 suggest that DolP is required to optimally survive the envelope modifications
185 consequent to activation of the $\sigma^E$ response in the corresponding deletion strains
186 [34,46,49]. This hypothesis is supported by the observation that $\sigma^E$ activation caused by
187 *rseA* silencing worsens the fitness of Δ*dolP* cells. We also noted that depletion of
188 the $\sigma^E$-dependent *micA* gene, which encodes a small antisense RNA that reduces
189 the expression of some OMPs during envelope stress, caused a negative fitness in
190 wild-type but not in Δ*dolP* cells (Tables S1 and S2). Although this CRISPRi hit
191 resulted from two independent experimental repeats, it is not highlighted in Figure
192 1C as the short nucleotide sequence of *micA* was targeted by only two sgRNAs (in

193 contrast to most genes that were targeted by 5 sgRNAs), and thus it was
194 considered as potentially non-significant by our statistical analysis. The fact that
195 Δ*dolP* tolerates lack of σE-dependent OMP downregulation would further support
196 the notion that the OMP assembly burden does not impair growth of this strain.

197 To further test the importance of DolP under envelope stress conditions, we
198 deleted *dolP* in a strain lacking *bamB,* which was identified with a lower genetic
199 score by the CRISPRi approach. In cells lacking BamB, the $\sigma^E$ response is partially
200 activated, causing the upregulation of *bam* genes (Fig. 2B). A strain carrying the
201 simultaneous deletion of *dolP* and *bamB* was viable but growth-defective (Fig. 2C).
202 Normal growth was restored by ectopic expression of a C-terminally, polyhistidine
203 tagged DolP protein variant (Fig. 2C). Phase-contrast analysis of the Δ*dolP* Δ*bamB*
204 strain revealed a number of cells with altered morphology or releasing vesicles as
205 well as several dead cells (Fig. 2D), indicating of a high degree of envelope stress
206 and possibly OM instability [50]. We conclude that although DolP is not crucial for
207 OMP biogenesis, its expression promotes optimal fitness probably by strengthening
208 OM integrity under the burden caused by envelope stress conditions and the
209 consequent $\sigma^E$-dependent response.

210

211 **DolP interacts with BamA assembled in the OM**

212 The observed interaction between *dolP* and *bam* genes prompted us to
213 investigate whether DolP physically interacts with the BAM complex. To this end, a
214 construct encoding C-terminally protein A-tagged DolP was ectopically
215 overproduced via the isopropylthiogalactoside (IPTG)-inducible *trc* promoter ($P_{trc}$).
216 The envelope of cells expressing $DolP^{ProtA}$ was solubilized using digitonin as main
217 mild-detergent component prior to IgG-affinity chromatography (Fig. 3A, coomassie
218 staining). Site-specific enzymatic cleavage of a protease-specific amino acid linker
219 between DolP and the protein A tag was used for protein elution. Notably, BamA,
220 BamC, BamD and BamE were immunodetected in the elution fraction of protein A-

221 tagged DolP (Fig. 3A, lane 3). In contrast, the inner membrane protein CyoA and
222 cytosolic RpoB were not detected. We next adapted a previously established
223 methodology and a $P_{trc}$-derivative construct [51] to ectopically overproduce $BAM^{ProtA}$
224 (consisting of wild-type BamABCD and a C-terminally protein A-tagged BamE
225 protein variant) and isolate the BAM complex via IgG-affinity purification.
226 Importantly, in addition to the BamE bait and other subunits of the BAM complex,
227 DolP was also immunodetected in the elution fraction (Fig. 3B, lane 3). Other
228 proteins of the bacterial envelope (Skp, OmpA, and $F_1\beta$ of the $F_1F_O$ ATP synthase)
229 or cytosolic RpoB were not detected (Fig. 3B). Taken together, our native pull-down
230 analysis indicates that DolP and BAM have affinity for each other.

231 To explore whether the central BAM subunit, BamA, is a critical determinant
232 of the BAM-DolP interaction, we performed Ni-affinity purification using the
233 solubilized envelope fraction obtained from cells overproducing BamA and C-
234 terminally polyhistidine-tagged DolP. Under these conditions, BamA was efficiently
235 co-eluted together with $DolP^{His}$, demonstrating that BamA and DolP can interact
236 even in the absence of stoichiometric amounts of the BAM lipoproteins (Fig. 3C,
237 coomassie staining). To assess if the interaction of DolP and BAM takes place at
238 the OM, $DolP^{His}$ was overproduced together with an assembly-defective form of
239 BamA, $BamA^{\Delta P1}$ [20]. When overproduced together with the BAM lipoproteins,
240 $BamA^{\Delta P1}$ largely accumulated in the periplasm, failing to efficiently assemble into
241 the BAM complex (Figs. S4A and S4B). When expressed together with $DolP^{His}$,
242 assembly-defective $BamA^{\Delta P1}$ was highly depleted in the corresponding eluate (Fig.
243 3C, lane 7), even though $BamA^{\Delta P1}$ was only marginally reduced in the crude
244 envelope fraction with respect to wild-type BamA (Fig. 3C, lane 3). In contrast to
245 $BamA^{\Delta P1}$, the $BamA^{\Delta P2}$ variant, which is efficiently assembled into the OM (Fig. S4),
246 was co-eluted with $DolP^{His}$ to a similar extent as wild-type BamA (Fig. 3C, lane 8).
247 This result indicates that DolP has affinity for OM-assembled BamA.

248 In seeking a detergent that would interfere with the interaction of BAM and
249 DolP, and allow their purification as separate components, we solubilized the
250 envelope fraction with increasing amounts of n-dodecyl β-D-maltoside (DDM), a
251 detergent previously used to isolate the native BAM complex [51]. At concentrations of
252 DDM between 0.3% (w/v) and 1% (w/v), we observed a drastic reduction in the
253 amounts of BAM subunits that were co-eluted with $DolP^{His}$ (Fig. 3D), indicating that
254 the BAM-DolP interaction is sensitive to DDM. We thus used 1% (w/v) DDM to
255 extract and purify His-tagged DolP or His-tagged BAM as separate components
256 (Fig. 3E). When analyzed by blue native-PAGE and immunoblotting, purified DolP
257 gave rise to a diffused signal at around 450 kDa (Fig. 3F, lane 1) suggesting a
258 dynamic multimeric organization of this protein. Purified BAM migrated as expected
259 at 250 kDa (Fig. 3F, lane 7). When purified BAM and DolP were pre-incubated in
260 the presence of a low DDM concentration and subsequently resolved by blue
261 native-PAGE, a complex with an apparent molecular weight higher than that of the
262 BAM complex was detected with both anti-BamA and anti-DolP specific antibodies
263 (Fig. 3F, lanes 3 to 6). Taken together our results demonstrate that the BAM
264 complex and DolP interact to form a larger complex and that OM-assembled BamA
265 is a critical determinant of this interaction. Only a portion of BAM and DolP
266 associate to form the BAM-DolP complex, indicating that the interaction is
267 substoichiometric.

268

269 **BamA overaccumulation in the OM reduces DolP mid-cell localization**

270 In light of our observation that DolP interacts with BAM, we asked whether
271 the envelope localization patterns of DolP and BAM are reciprocally linked. First, we
272 monitored the effect of DolP expression on the localization of the chromosomally
273 encoded $BamD^{mCherry}$ subunit of the BAM complex. This protein generated a
274 fluorescence signal throughout the envelope that was not affected by the lack or the
275 overproduction of DolP (Fig. S5). Next, we checked the effect of BAM

276 overaccumulation in the OM on DolP localization. DolP associates with the OM and
277 accumulates at mid-cell during a late step of cell division [33]. To monitor the
278 localization of DolP, we used a strain harbouring a chromosomal *dolP-gfp* fusion
279 (Fig. 1A). The localization of the DolP$^{GFP}$ fusion protein (Fig. S6A) was analyzed
280 concomitantly to other two chromosomally-encoded markers of the division septum,
281 ZipA$^{mCherry}$ or NlpD$^{mCherry}$. ZipA is involved in an early step of divisome assembly
282 and accumulates at division sites before, as well as, during envelope constriction
283 (Fig. S6B) [52]. Instead, NlpD is a late marker of cell division involved in the activation
284 of AmiC and accumulates at septa that are already undergoing constriction (Fig.
285 S6C)[42,44]. DolP$^{GFP}$ accumulated at mid-cell sites where the envelope appeared
286 invaginated, showing a localization pattern similar to that of NlpD$^{mCherry}$ (Fig. S6C)
287 [33]. Strikingly, we found that ectopic BAM overproduction (Fig. S7A) depleted
288 DolP$^{GFP}$ from mid-cell sites (Fig. 4A, center). In contrast, no obvious effects on cell
289 division nor on mid-cell recruitment of ZipA$^{mCherry}$ and NlpD$^{mCherry}$ was observed (Fig.
290 S7B). The depletion of DolP at mid-cell sites was dependent on BamA
291 overaccumulation, as the overproduction of only the four BAM lipoproteins did not
292 prevent DolP$^{GFP}$ mid-cell localization (Fig. 4A, right). In another control experiment,
293 we observed that the overproduction of a different OM-spanning protein, OmpA, did
294 not prevent DolP mid-cell localization (Fig. S7C). To check whether the OMP-
295 biogenesis activity of BamA impairs DolP mid-cell localization, we made use of an
296 inactive BamA mutant form (Fig. S8A) harbouring a polyhistidine peptide extension
297 at its C-terminal β-strand[53]. Similar to the overaccumulation of the full BAM
298 complex, the overaccumulation of BamA$^{His}$ interfered with DolP mid-cell localization
299 (Figs. S8B and S8C), without affecting ZipA$^{mCherry}$ and NlpD$^{mCherry}$ (Fig. S7D),
300 indicating that the cellular localization of DolP does not depend on the OMP-
301 assembly activity of BamA. In contrast, the ability of BamA to assemble into the OM
302 was a critical determinant of the observed septal depletion of DolP. In fact, the
303 periplasm-accumulating BamA$^{\Delta P1/His}$ variant (Fig. S8D) did not impair DolP$^{GFP}$ mid-
304 cell localization (Fig. S8B, center), whereas the OM-overaccumulating BamA$^{\Delta P2/His}$

305 did (Figs. S8B, right, S8C, and S8D). Taken together, these results suggest that the
306 overaccumulation of BamA in the OM interferes with the recruitment of DolP at mid-
307 cell sites.

308

309 **DolP mid-cell localization is impaired under envelope stress conditions**

310 Because we observed that DolP is critical for fitness under envelope stress
311 conditions, we asked whether the localization of DolP$^{GFP}$ would be affected in
312 mutants than manifest envelope stress. To this end, we analyzed the localization of
313 DolP$^{GFP}$ in strains lacking either the OMP chaperone SurA or the lipoprotein BamB.
314 Both Δ*surA* and Δ*bamB* strains have an enhanced OM permeability and produce
315 higher levels of BAM complex due to activation of the $\sigma^E$ response [49,54] (Fig. 2B).
316 Importantly, the frequency of mid-cell labelling by DolP$^{GFP}$ was reduced by more
317 than half in Δ*surA* cells (Fig. 4B). As observed for the Δ*surA* strain, DolP$^{GFP}$
318 accumulated at the mid-cell with a lower frequency also when *bamB* was deleted
319 (Fig. S8E). Together, our results indicate that the depletion of DolP at mid-cell sites
320 occurs during the physiological response to conditions that cause envelope stress.

321

322 **Discussion**

323 Despite its importance in maintaining OM integrity, the reason why DolP is
324 upregulated by $\sigma^E$ has remained unknown [32-34]. Here we demonstrate an
325 unprecedented interaction of DolP with the BAM complex. Differently from other
326 factors upregulated upon $\sigma^E$ activation, DolP does not directly promote OMP
327 biogenesis. Instead, DolP is crucial for fitness in cells with elevated $\sigma^E$ activity and
328 its cell localization is sensitive to envelope stress as well as to the overaccumulation
329 of BAM in the OM. Our results have important implications for the understanding of
330 the mechanisms that coordinate OM and peptidoglycan remodelling and that help
331 preserving envelope integrity.

332 We have obtained several pieces of evidence suggesting that DolP is not
333 strictly required for OMP assembly into the OM under our experimental conditions.
334 Lack of DolP, in fact, does not reduce the steady state levels of OMPs, nor it
335 impairs the kinetics of assembly of an autotransporter virulence factor. Furthermore,
336 we could not detect activation of the $\sigma^E$ response in cells lacking DolP. Activation of
337 $\sigma^E$ has been reported to alleviate defects caused by lack or inactivation of OMP
338 biogenesis factors [55-58]. On the contrary, activation of $\sigma^E$ caused a fitness defect in a
339 Δ*dolP* strain. This result suggests that, under envelope stress conditions, DolP
340 plays a role different from OMP assembly and probably only indirectly related to
341 OMP biogenesis. In this respect, it is notable that the CRISPRi screen highlighted a
342 synthetic defect caused by lack of DolP and depletion of the Sec ancillary complex
343 SecDF-YajC, which is important for secretion of proteins across the inner
344 membrane, including OMPs [22]. Trans-envelope interactions of this complex with
345 BAM have been proposed to optimize the flux of unfolded OMPs across the
346 periplasm [47,48]. It is thus likely that conditions causing a depletion of OMPs in the
347 OM are particularly detrimental in cells lacking DolP.

348 Although the details of how DolP contributes to maintain OM integrity and
349 how it supports growth under envelope stress conditions will warrant further studies,
350 it is worth noting that DolP consists of two BON (bacterial OsmY and nodulation)
351 domains, folding motifs predicted to interact with hydrophobic ligands such as lipids
352 [59]. Phospholipid-binding by DolP has been reported in a recent study [60]. Two
353 aspects of our results hint at a plausible role of the lipid-binding function of DolP in
354 promoting fitness during envelope stress. The first is related to the biochemical
355 interaction of DolP with the BamA subunit of the BAM complex, which is predicted
356 to locally interfere with the organization of the OM lipid bilayer and to generate an
357 energetically favourable environment for the insertion of nascent OMPs [61,62]. BamA-
358 mediated membrane destabilization was shown by molecular dynamics simulations,
359 as well as by reconstituting BamA into proteoliposomes [9,63]. Thus, it is possible that

360 during envelope stress the increased amount of BamA has an impact on the
361 organization of the OM and contributes to some degree to the described detrimental
362 effect of elevated $\sigma^E$ activity [30,31]. It remains to be seen how DolP docks to BamA,
363 and whether it influences the organization of BAM sites and of the surrounding lipid
364 bilayer. The second aspect consists in *dolP* being a fitness factor in cells with an
365 active $\sigma^E$ response and reduced OMP biogenesis. OMPs represent a major
366 component of the OM and are likely to occupy nearly half of its surface[62]. OMPs are
367 largely arranged in clusters [64-66] embedded by highly organized LPS molecules in
368 the external leaflet of the OM [4] and the rigidity of their β-barrel structures contributes
369 to the mechanical stiffness of the OM [67]. The importance of OMPs for OM integrity
370 is highlighted by the fact that mutant strains lacking some of the major OMP
371 components (OmpA, OmpC and OmpF) present an enhanced OM permeability to
372 several antibiotics and detergents [30,68]. We propose that DolP plays a role in
373 preserving the structure of the OM, when BAM and OMP levels are inversely altered
374 by the activation of the $\sigma^E$ transcriptional response [25,54].

375 Another key result that emphasizes the importance of DolP during envelope
376 stress is the observation that septal localization of DolP is impaired under this
377 condition. Distinct biogenesis and surveillance pathways are required to maintain
378 the protective function of the multi-layered envelope of Gram-negative bacteria.
379 Emerging evidence is uncovering an intricate trans-envelope network of protein-
380 protein interactions that connect biogenesis machineries, stress-sensing factors and
381 their associated transducing pathways across the envelope layers [2,47,69-71]. DolP
382 septal localization was shown to be critical for efficient NlpD-mediated activation of
383 AmiC during septal peptidoglycan splitting [33]. Cells lacking both NlpD and AmiC
384 have reduced OM integrity [33], which may contribute to explain the vancomycin
385 sensitivity of Δ*dolP* cells. It is however unknown whether envelope stress caused by
386 the accumulation of unfolded OMPs influences peptidoglycan remodelling.
387 Intriguingly, our observation that mid-cell localization of DolP is reduced in *surA* or

388 *bamB* deletion mutant strains points to a role of DolP in linking envelope stress to
389 septal peptidoglycan hydrolysis. Whereas we have demonstrated that the
390 overaccumulation of BamA in the OM impairs the recruitment of DolP to the mid-
391 cell, it is possible that also other envelope features that are modified under
392 envelope stress conditions, for instance as a consequence of OMP depletion,
393 contribute to influence DolP localization. We suggest that reduced levels of DolP at
394 mid-cell sites, and thus impaired AmiC activation [33], can play an important role in
395 coping with envelope stress, for instance by regulating the window of time available
396 to restore normal OMP biogenesis prior to completing the formation of the new
397 poles in the cell offspring.
398

399 **Materials and Methods**

400 **Bacterial strains and growth conditions**

401 All *E. coli* strains used in this study are listed in Table S3. Strains newly
402 generated for this study derive from BW25113 [Δ(*araD-araB*)*567* Δ(*rhaD-rhaB*)*568*
403 Δ*lacZ4787* (::rrnB-3) *hsdR514 rph-1*] [72] or MG1655 ($F^-$ $\lambda^-$ *ilvG*$^-$ *rfb-50 rph-1*) [73].
404 Deletions of *dolP*, *envC*, *rseA, surA,* or *bamB* in a BW25113 strain was achieved by
405 P1 transduction of the Δ*dolP::kan*$^R$, Δ*envC::kan*$^R$, Δ*rseA::kan*$^R$, Δ*surA::kan*$^R$ and
406 Δ*bamB::kan*$^R$ alleles, respectively, obtained from the corresponding Keio collection
407 strains [37]. BW25113 derivative strains harbouring chromosomal fusions of
408 constructs encoding superfolder GFP downstream of *dolP* or mCherry downstream
409 of *nlpD*, *zipA* and *bamD* were obtained by λ-red recombination as previously
410 described [74]. Briefly, a kanamycin-resistance cassette was amplified from plasmid
411 pKD4 using oligonucleotides carrying extensions of approximately 50 nucleotides
412 homologous to regions immediately upstream or downstream the stop codon of the
413 interested gene. *Dpn*I-digested and purified PCR products were electroporated into
414 the BW25113 or derivative strains. Recombinant clones were selected at 37°C on
415 LB agar plates containing kanamycin. When necessary, the *kan*$^R$ cassette inserted
416 into a mutated locus (gene deletion or fusion) was removed upon transformation
417 with the heat-curable plasmid pCP20 [74]. The MG1655 derivative strain, LC-E75,
418 harbouring a dCas9-encoding construct under the control of the $P_{tet}$ promoter has
419 been described [38]. Cells were cultured in home-made lysogeny broth (LB) medium
420 (1% (w/v) tryptone, 0.5% (w/v) yeast extract, 5 mg/ml (NaCl), commercially
421 available Miller LB Broth (Sigma) or M9 minimal medium containing M9 salts (33.7
422 mM $Na_2HPO_4$, 22 mM $KH_2PO_4$, 8.55 mM NaCl, 9.35 mM $NH_4Cl$) and supplemented
423 with 0.2% w/v glycerol and all the amino acids, or all amino acids except methionine
424 and cysteine in the case of $^{35}S$ pulse-chase labeling. Antibiotics were used at the
425 following concentrations: ampicillin 100 μg/ml, kanamycin 50 μg/ml, vancomycin 60

426 μg/ml. For spot tests, cells were cultured to mid-log phase, washed with M9 salts
427 and serially diluted in ice-cold M9 salts prior to spotting on agar plates.

428

429 **Plasmid construction**

430 All plasmids used in data figures are listed in Table S4. Plasmids for the
431 ectopic expression of BAM subunits, DolP, or OmpA are derived from a pTRC99a
432 vector. The plasmid pBAM$^{His}$ (pJH114), which harbours a $P_{trc}$ promoter followed by
433 the *bamABCDE* open reading frames and an octahistidine tag fused downstream of
434 *bamE* was described [51]. The region of pBAM$^{His}$ comprising the segment that spans
435 from the *bamA* start codon to the *bamE* stop codon was deleted by site-directed
436 mutagenesis, generating pCtrl. Plasmids pBamA$^{His}$ was generated by restriction-
437 free cloning inserting the *bamA* ORF without its stop codon downstream of the $P_{trc}$
438 promoter and upstream of the octahistidine encoding region in pCtrl. The *dolP* ORF
439 amplified from the BW25113 genomic DNA was used to replace the *bamABCDE*
440 ORFs in pJH114 by restriction-free cloning, generating pDolP$^{His}$. The plasmid
441 pBamA-DolP$^{His}$ was generated by restriction-free cloning of the *bamA* ORF between
442 the $P_{trc}$ promoter and *dolP* in pDolP$^{His}$. Site-directed mutagenesis was conducted on
443 pBAM$^{His}$ (pJH114) to obtain pBamBCDE$^{His}$. A sequence encoding the tobacco etch
444 virus protease cleavage site (TEV site) followed by a tandem Protein-A tag was
445 amplified from pYM10 [75] and fused by restriction-free cloning with the last codon of
446 the *bamE* gene in pBAM$^{His}$ to generate pBAM$^{ProtA}$. A stop codon was introduced
447 downstream of the *bamE* last codon to generate pBAM. Plasmids encoding the ΔP1
448 and ΔP2 BamA variant were obtained by site-directed mutagenesis deleting the
449 portion of *bamA* ORFs corresponding to residues E22-K89 or P92-G172,
450 respectively. The TEV site and the tandem Protein-A construct amplified from
451 pYM10 was inserted by restriction-free cloning downstream of the *dolP* last codon in
452 pDolP$^{His}$, generating pDolP$^{ProtA}$. pDolP was derived from pDolP$^{ProtA}$ using site-
453 directed mutagenesis to introduce a stop codon immediately downstream of the

454 *dolP* ORF. The *ompA* ORF was amplified from the BW25113 genomic DNA and
455 inserted by restriction-free cloning between Ptrc and the His-tag encoding construct
456 of pCtrl to generate pOmpA$^{His}$. The sgRNAs plasmids are derived from psgRNAcos
457 [38]. To generate sgRNA-encoding plasmids the DNA sequences
458 AGCTGCACCTGCTGCGAATA (*bamD* sgRNA, plasmid pCAT187),
459 GTAAACCACTCGCTCCAGAG (*bamE* sgRNA, plasmid pCAT189),
460 CTCATCCGCGTGGGCGGAAA (*envC* sgRNA, plasmid pCAT191), and
461 CTGAGCCGCCGACCGATTTA (*ftsX* sgRNA, pCAT193) were inserted into a *Bsa*I
462 site of the psgRNAcos.

463

464 **CRISPRi screen and data analysis**

465 Strain LC-E75 (*dolP*$^{+}$) and its Δ*dolP* derivative were transformed with the
466 EcoWG1 library which contains 5 guides per gene as previously described [39]. After
467 culturing pooled transformant cells in LB at 37°C to early exponential phase (optical
468 density at 600 nm [$OD_{600}$] = 0.2), a sample was withdrawn for plasmid isolation
469 ($t_{start}$). Subsequently, cultures were supplemented with 1 μM anhydrotetracycline
470 (aTc) to induce dCas9 expression and further incubated at 37°C. When cultures
471 reached an $OD_{600}$ of 2 they were diluted 1:100 into LB supplemented with 1 μM aTc
472 and incubated at the same temperature until an $OD_{600}$ of 2. This step was repeated
473 one more time prior to withdrawing a sample for isolation of plasmid DNA ($t_{end}$).
474 Sequencing indexes were used to assign reads to each sample. Illumina
475 sequencing samples were prepared and analyzed as previously described [38].
476 Briefly, a two-step PCR was performed with Phusion polymerase (Thermo
477 Scientific) using indexed primers. The first PCR adds the first index and the second
478 PCR adds the second index and flow-cell attachment sequences. Pooled PCR
479 products were gel-purified. Sequencing was performed on a NextSeq550 machine
480 (Illumina). The total number of reads obtained for each sample was used to
481 normalize raw reads by sample size. Replicates were pooled to increase depth

482 before another normalization by sample size. Guides with less than 100 normalized
483 read counts in initial time points were discarded. For each screen, sgRNA fitness
484 was calculated as the log2-transformed ratio of normalized reads counts between
485 the final and the initial time point:

486 $$log2FC = log2\left(\frac{Normalized\ reads_{final} + 1}{Normalized\ reads_{initial} + 1}\right)$$

487 For each sample, log2FC values were centered by subtracting the median log2FC
488 of non-targeting control guides. We then calculated for each sgRNA the difference
489 of log2FC value between the Δ*dolP* screen and the *dolP*$^+$ screen. Guides were
490 ranked from the lowest negative values (negative fitness effect in Δ*dolP* compared
491 to *dolP*$^+$) to the highest positive values (positive fitness effect in Δ*dolP* compared to
492 *dolP*$^+$) and the significance of the interaction between *dolP* and each gene was
493 evaluated by performing a minimum hypergeometric (mHG) test on the ranked list
494 for each gene using the mHG R package (v. 1.1) [76]. False-discovery rate (FDR) was
495 used to correct p-values for multiple testing. For each gene, the median difference
496 of log2FC between Δ*dolP* and *dolP*$^+$ screens was used as a measure of the genetic
497 interaction.

498

499 **Cell fractionation**

500 To prepare whole-cell lysates, cells were cultured to early exponential phase
501 ($OD_{600}$ = 0.2-0.3) in LB medium at 37°C and collected. Where indicated, IPTG was
502 added 30 min prior to cell collection. Cells were pelleted by centrifugation, washed
503 once with M9 salt and lysed with Laemmli Sample Buffer (BioRad) (69 mM Tris-HCl,
504 pH 6.8, 11.1% [v/v] glycerol, 1.1% [w/v] lithium dodecyl sulfate [LDS], 0.005% [w/v]
505 bromophenol blue, supplemented with 357 mM β-mercaptoethanol and 2 mM
506 phenylmethylsulfonyl fluoride [PMSF]). The total protein content was denatured at
507 98°C for 5 min prior SDS-PAGE analysis.

508 To perform lysozyme/EDTA lysis, cells were cultured to early exponential phase,
509 collected by centrifugation, resuspended in 33 mM Tris-HCl pH 8 to an $OD_{600}$ of 1.
510 The cell suspension was then supplemented with 0.1 mg/ml lysozyme (Sigma), 2
511 mM EDTA and incubated on ice for 20 minutes to induce lysis. After addition of 10
512 mM $MgSO_4$, the membrane fraction was collected by centrifugation at 16000x *g*. The
513 supernatant was further centrifuged at 100000x *g* to remove any residual
514 membrane fraction, which was discarded. The obtained soluble fraction was
515 subjected to protein precipitation by adding 10% (w/v) trichloroacetic acid (TCA).
516 TCA precipitates were solubilized in Laemmli Sample Buffer prior to SDS-PAGE
517 analysis.

518 The crude envelope fraction used for native affinity purification of affinity
519 tagged BAM complex or DolP was prepared from cells that were cultured in LB until
520 an $OD_{600}$ of approximately 0.25 and then supplemented with 400 μM IPTG for 1
521 hour to induce ectopic expression. Cells were collected by centrifugation at 6000x *g*
522 at 4°C, resuspended in 20 mM Tris-HCl pH 8, and mechanically disrupted using a
523 Cell Disruptor (Constant Systems LTD) set to 0.82 kPa. The obtained cell lysate
524 fractions were clarified by centrifugation at 6000x *g* and 4°C. The supernatant was
525 then subjected to ultracentrifugation at 100000x *g* at 4°C to collect the envelope
526 fraction.

527

528 **Isolation of native protein complexes by IgG- or nickel-affinity**
529 **chromatography**

530 The envelope fraction was resuspended at a concentration of approximately
531 10 mg/ml in solubilization buffer (20 mM Tris-HCl pH 7.4, 100 mM NaCl, 0.1 mM
532 EDTA, 2 mM PMSF) supplemented with EDTA-free protease inhibitor cocktail
533 (Roche), and 1.1% (w/v) of a mild detergent component corresponding to digitonin
534 (Merck) and n-dodecyl β-D-maltoside (DDM, Merck) as indicated in Figure Legends.
535 To facilitate extraction of membrane proteins, samples were subjected to mild

536 agitation for 1 hour at 4°C. Insoluble material was removed by centrifugation at
537 16000x *g* at 4°C. To perform IgG affinity purification, membrane-extracted proteins
538 were incubated for 1.5 hours at 4°C with purified human IgG (Sigma) that had been
539 previously coupled to CNBr-activated Sepharose beads (GE Healthcare). After
540 extensive washes of the resin with solubilization buffer containing 0.3% (w/v)
541 digitonin and 0.03% (w/v) DDM, bound proteins were eluted by incubation with
542 AcTEV protease (ThermoFisher) overnight at 4°C under mild agitation. To perform
543 nickel (Ni)-affinity purification, membrane-extracted proteins were supplemented
544 with 20 mM imidazole and incubated with Protino Ni-NTA agarose beads
545 (Macherey-Nagel) for 1 hour at 4°C. After extensive washes of the resin with
546 solubilization buffer supplemented with 50 mM imidazole, 0.3% (w/v) digitonin,
547 0.03% (w/v) DDM, and the EDTA-free protease inhibitor cocktail (Roche), bound
548 proteins were eluted using the same buffer supplemented with 500 mM imidazole.

549

550 ***In vitro* reconstitution of the BAM-DolP interaction and BN-PAGE analysis**

551 Envelope fractions were obtained from cells carrying pBAM$^{His}$ or pDolP$^{His}$
552 and cultured until early exponential phase in LB medium at 37°C and subsequently
553 supplemented with 400 μM IPTG for 1.5 hours to induce the expression of the BAM
554 complex genes or *dolP*. The envelope fractions were solubilized and purified by Ni-
555 affinity and size exclusion chromatography, adapting a previously published
556 protocol. Briefly, after membrane solubilization with 50 mM Tris-HCl pH 8.0, 150
557 mM NaCl, and 1% (w/v) DDM, and removal of insoluble material by
558 ultracentrifugation at 100000x *g*, 4°C, soluble proteins were loaded onto a Ni-
559 column (HisTrap FF Crude, GE Healthcare) pre-equilibrated with 50 mM Tris-HCl
560 pH 8.0, 150 mM NaCl, and 0.03% (w/v) DDM (equilibration buffer), using an ÄKTA
561 Purifier 10 (GE Healthcare) at 4°C. The column containing bound proteins was
562 washed with equilibration buffer supplemented with 50 mM imidazole. Proteins were
563 eluted in equilibration buffer, applying a gradient of imidazole from 50 mM to 500

564 mM and further separated by gel filtration using an HiLoad 16/600 Superdex 200
565 (GE Healthcare) in equilibration buffer. Eluted proteins were concentrated using an
566 ultrafiltration membrane with a 10 kDa molecular weight cutoff (Vivaspin 6,
567 Sartorius). To reconstitute the BAM-DolP complex *in vitro,* equimolar concentrations
568 of purified BAM and DolP were used. Purified proteins were mixed in equilibration
569 buffer for 1 hour at 4°C or for 30 min at 25°C as indicated in Figure Legends. The
570 reaction was further diluted 1:4 times in ice-cold blue native buffer (20 mM Tris-HCl
571 pH 7.4, 50 mM NaCl, 0.1 mM EDTA, 1% [w/v] digitonin, 10% w/v glycerol) and ice
572 cold blue native loading buffer (5% coomassie brilliant blue G-250, 100 mM Bis-
573 Tris-HCl, pH 7.0, 500 mM 6-aminocaproic acid) prior to loading onto home-made 5-
574 13% blue native polyacrylamide gradient gels. Resolved protein complexes were
575 blotted onto a PVDF membrane and immunodecorated. Where non-relevant gel
576 lanes were removed, a white space was used to separate contiguous parts of the
577 same gel.

578

579 **Pulse-chase *in vivo* protein labeling**

580 Pulse-chase labeling of cellular proteins with radioactive $^{35}$S methionine and
581 cysteine was conducted as previously described [77]. Briefly, overnight cultures were
582 washed and freshly diluted into M9 medium to $OD_{600}$ = 0.03 and incubated at 37 °C.
583 When the cultures reached $OD_{600}$ = 0.3, ectopic expression of EspP was induced by
584 adding 200 µM IPTG for 30 min. $^{35}$S labelling was performed by supplementing
585 cultures with a mixture of [$^{35}$S]-methionine and [$^{35}$S]-cysteine followed after 30
586 seconds by the addition of an excess of cold methionine and cysteine. Samples
587 were withdrawn at different chase times, immediately mixed with ice and subjected
588 to TCA precipitation, prior to immunoprecipitation.

589

590 **Antibodies**

591 Proteins separated by SDS-PAGE or blue native-PAGE and blotted onto
592 PVDF membranes were immunodecorated using epitope-specific rabbit polyclonal
593 antisera with the following exceptions. The $F_1\beta$ subunit of the ATP $F_1F_O$ synthase
594 was detected using a rabbit polyclonal antiserum raised against an epitope of the
595 homologous protein of Saccharomyces cerevisiae (Atp2). RpoB was detected using
596 a mouse monoclonal antibody (NeoClone Biotechnology). The secondary
597 immunodecoration was conducted using anti-rabbit or anti-mouse peroxidase-
598 conjugated antibodies produced in goat (Sigma). EspP immunoprecipitation was
599 conducted using a rabbit polyclonal antiserum specific for a C-terminal epitope of
600 EspP.

601

602 **Epifluorescence microscopy and analysis**

603 Overnight cultures of *E. coli* BW25113 and its derivative strains were diluted
604 into fresh M9 medium containing 0.2% glycerol and grown at 30°C to $OD_{600}$ = 0.2-
605 0.3. When indicated, cultures were supplemented with 400 μM of IPTG to induce
606 ectopic expression of plasmid-borne genes for at least 1 hour prior to collecting
607 samples for microscopy analysis. Culture volumes of 0.6 μl were deposited directly
608 onto slides coated with 1% (w/v) agarose in a phosphate-buffered saline solution
609 and visualized by epifluorescence microscopy. Cells were imaged at 30°C using an
610 Eclipse TI-E/B Nikon wide field epifluorescence inverted microscope with a phase
611 contrast objective (Plan APO LBDA 100X oil NA1.4 Phase) and a Semrock filter
612 mCherry (Ex: 562BP24; DM: 593; Em: 641BP75) or FITC (Ex: 482BP35; DM: 506;
613 Em: 536BP40). Images were acquired using a CDD OrcaR2 (Hamamatsu) camera
614 with illumination at 100% from a HG Intensilight source and with an exposure time
615 of 1-3 seconds. Nis-Elements AR software (Nikon) was used for image capture.
616 Image analysis was conducted using the Fiji software. Counting of cells with
617 $DolP^{GPF}$ signals at mid-cell sites was performed using the Fiji Cell Counter plugin.

618

## Acknowledgments

We thank Harris Bernstein (NIDDK/NIH, Bethesda, MD) for providing key reagents and for comments on the manuscript. We thank Tanneke Den Blaauwen (University of Amsterdam) and Nathalie Dautin (IBPC/CNRS, Paris) for discussion. We thank the Light Imaging Toulouse CBI (LITC) platform for assistance with and maintenance of the microscopy instrumentation. Financial support was provided by: the Fondation pour la Recherche Médicale to D.R.; the Chinese Scholarship Council to Y.Y.; the Ecole Normale Supérieure to F.R.; the European Research Council (Europe Union's Horizon 2020 research and innovation program, grant agreement No 677823), the French governmental Investissement d'Avenir program and the Laboratoire d'Excellence "Integrative Biology of Emerging Infectious Diseases" (ANR-10-LABX-62-IBEID) to D.B.; the CNRS ATIP-Avenir program to R.I.

## Author contribution

R.I. conceived the project and wrote the manuscript; D.B. conceived and developed the CRISPRi approach; R.I., D.B., D.R. L.C. and C.A. supervised the experiments; D.R., Y.Y., L.O., F.R., L.C., V.M., C.M., G.M., A.C.-S, C.T., J.R. and C.A. performed the experiments and analyzed the data together with R.I. and D.B.; A.C.-S, D.R., Y.Y., L.O. and F.R. prepared the figures; all authors discussed the project and the experimental results, and commented on the manuscript.

642 **Figures and Figure Legends**

643

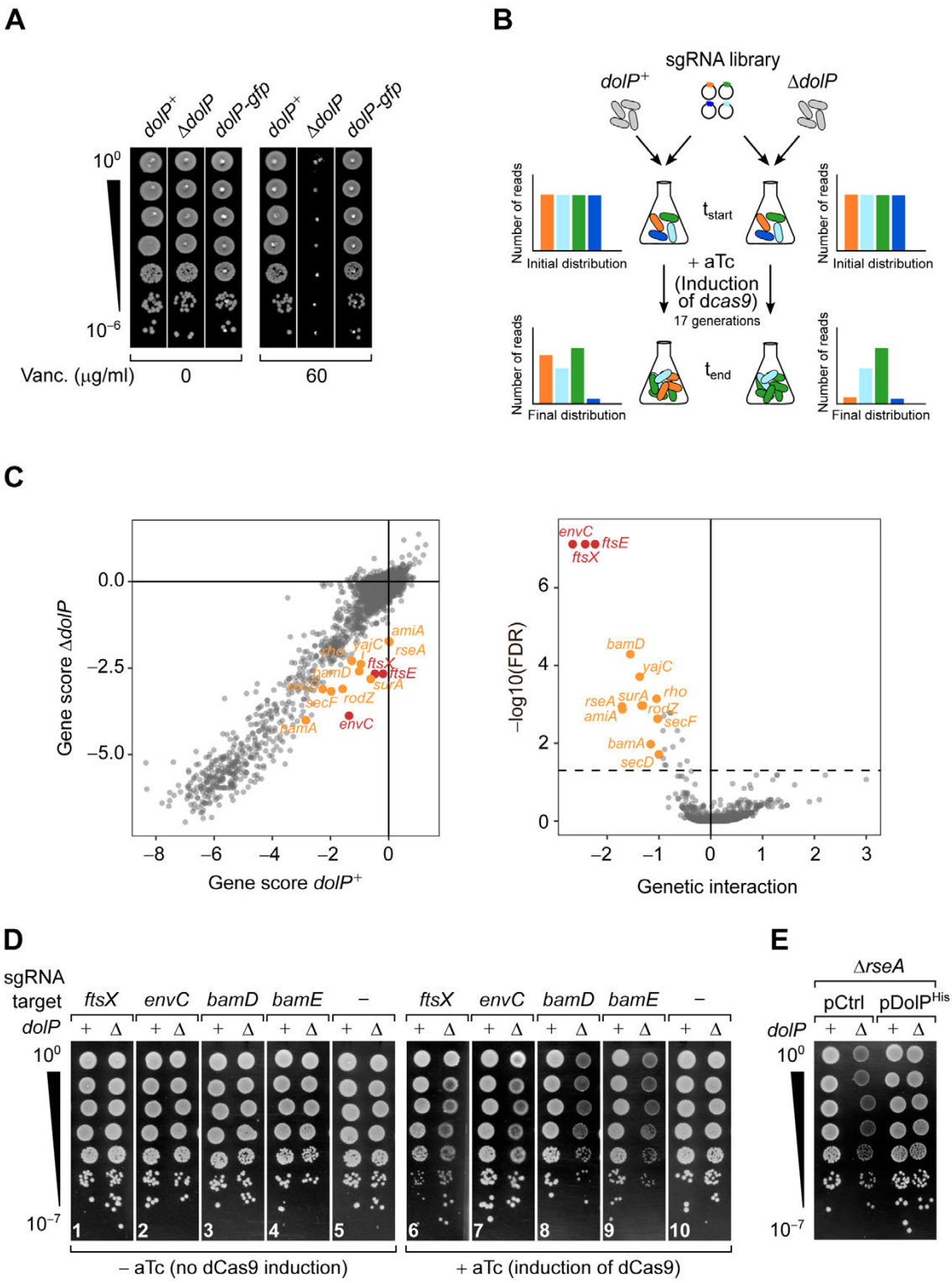
A
dolP+
ΔdolP
dolP-gfp
dolP+
ΔdolP
dolP-gfp
10^0
10^−6
Vanc. (μg/ml)
0
60
B
sgRNA library
dolP+
ΔdolP
Number of reads
Initial distribution
t start
+ aTc
(Induction
of dcas9)
17 generations
t end
Final distribution
C
Gene score ΔdolP
Gene score dolP+
amiA
yajC
rseA
rho
ftsX
bamD
ftsE
surA
secD
secF
rodZ
bamA
envC
−log10(FDR)
Genetic interaction
D
sgRNA target
ftsX
envC
bamD
bamE
–
dolP
+
Δ
10^0
10^−7
1
2
3
4
5
6
7
8
9
10
– aTc (no dCas9 induction)
+ aTc (induction of dCas9)
E
ΔrseA
pCtrl
pDolP His

**Figure 1.**

644

645 **Fig. 1. Genome-wide screen of *dolP* interactions.**

646 (**A**) The deletion of *dolP* impairs OM integrity. The indicated strains were serially
647 diluted and spotted onto LB agar plates lacking or supplemented with 60 μg/ml
648 vancomycin as indicated.

649 (**B**) Schematic representation of the CRISPR-based gene silencing approach. LC-
650 E75 (*dolP*$^+$) or its Δ*dolP* derivative strain, both carrying d*cas9* under the control of
651 an anhydrotetracycline (aTc)-inducible promoter in their chromosome were
652 transformed with a library of plasmids encoding gene-specific sgRNAs. The library
653 covers any *E. coli* MG1655 genetic features with an average of 5 sgRNAs per gene.
654 Pooled transformed cells were cultured to early exponential phase prior to plasmid
655 extraction and quantitative Illumina sequencing to assess the initial distribution of
656 sgRNA constructs in each culture ($t_{start}$). Upon addition of 1 μM aTc to induce
657 sgRNA-mediated targeting of d*cas9* for approximately 17 generations, samples of
658 cells from each culture were newly subjected to plasmid extraction and Illumina
659 sequencing to determine the final distribution of sgRNA constructs ($t_{end}$).

660 (**C**) Left: Comparison of gene scores obtained in *dolP*$^+$ and Δ*dolP* screens. The log2
661 fold-change (log2FC) between $t_{end}$ and $t_{start}$ calculated for each sgRNAs (Fig. S2B)
662 was grouped by gene target, and their median (Table S1) was used to derive fitness
663 gene scores. Right: Volcano plot of the *dolP* genetic interaction (GI) scores. The x-
664 axis shows a genetic interaction score calculated for each gene based on the
665 minimum hypergeometric (mHG) test conducted on the ranked difference of
666 sgRNA-specific log2FC values between the Δ*dolP* and the *dolP*$^+$ screens. The y-
667 axis shows the log10 of the false discovery rate FDR of the test. The dashed line
668 shows FDR = 0.05. In both panels, genes highlighted in orange have FDR < 0.05
669 and GI>1 whereas genes highlighted in red have FDR < 0.05 and GI>2.

670 (**D** and **E**) Validation of the genetic interactions determined in (C). (D) LC-E75
671 (*dolP*$^+$) or its Δ*dolP* derivative strain expressing sgRNAs that target the indicated
672 genes were serially diluted and spotted on LB agar lacking or supplemented with

673 aTc to induce expression of d*cas9*, as indicated. (E) BW25113 derivative cells
674 deleted of *rseA* or both *rseA* and *dolP* were transformed with an empty vector
675 (pCtrl) or a plasmid encoding DolP (pDolP$^{His}$). Ectopic expression of DolP$^{His}$ was
676 driven by the leaky transcriptional activity of $P_{trc}$ in the absence of IPTG. (D and E)
677 10-fold serial dilutions of the indicated transformants were spotted on LB agar.
678

679

680

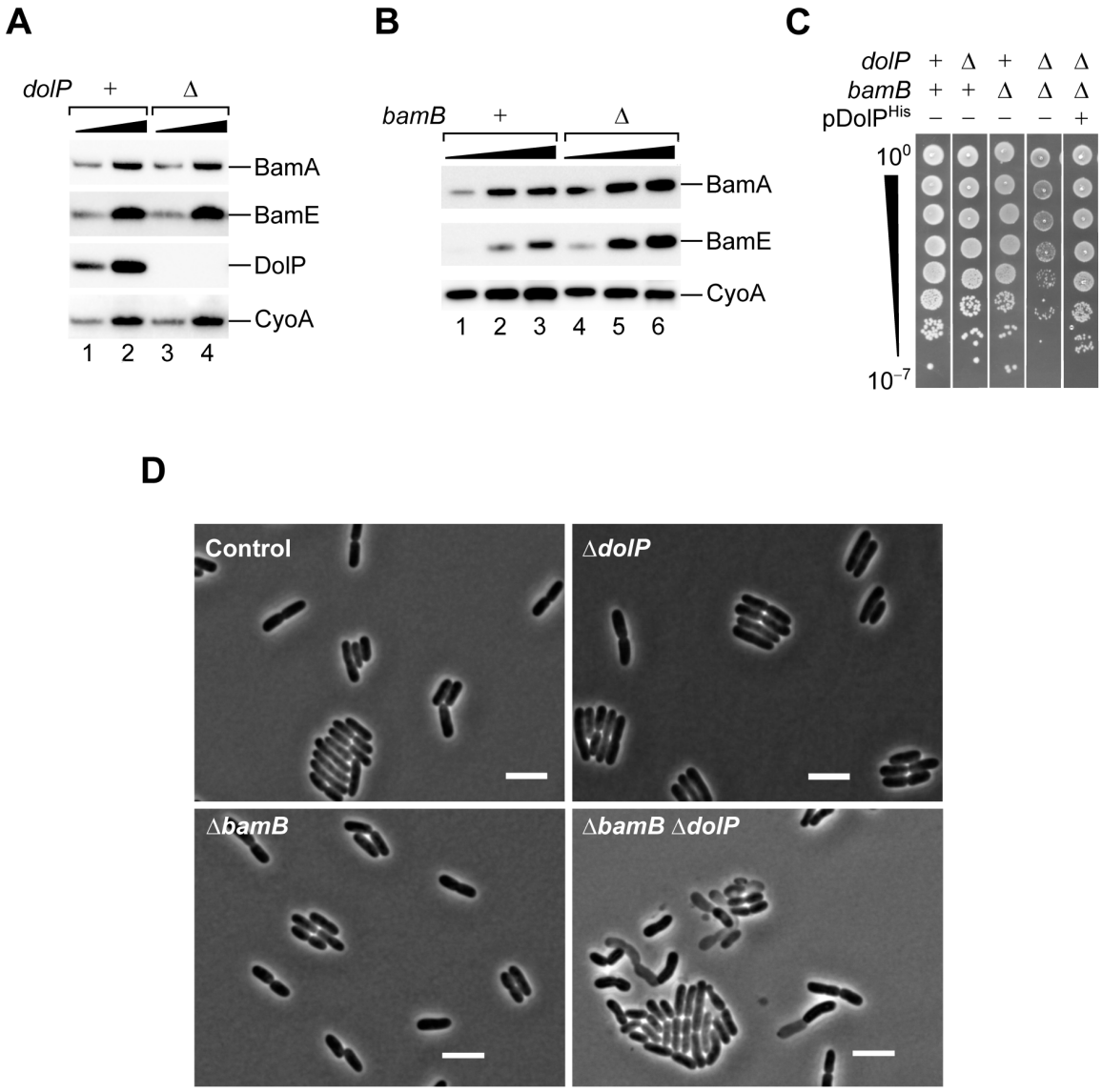


**Figure 2.**

681

682 **Fig. 2. DolP promotes fitness under envelope stress conditions.**

683 (A) One and three folds of a sample containing the total cell lysate fraction from a
684 BW25113 (*dolP*$^{+}$) strain and a derivative Δ*dolP* strain were analyzed by SDS-PAGE
685 and immunoblotting using the indicated antisera.

686 (B) One, two and three folds of a sample containing the total cell lysate fraction from
687 a BW25113 (*bamB*$^{+}$) strain and a derivative Δ*bamB* strain were analyzed by SDS-
688 PAGE and immunoblotting using the indicated antisera.

689 (C) BW25113 and derivative cells deleted of *dolP, bamB* or both genes were
690 cultured, serially diluted and spotted on LB agar. A BW25113 derivative strain
691 deleted of both *dolP* and *bamB* was cultured, serially diluted and spotted on LB agar
692 supplemented with ampicillin.

693 (D) Overnight cultures of BW25113 (control), Δ*dolP,* Δ*bamB and* Δ*dolP* Δ*bamB,*
694 were freshly diluted in LB medium and re-incubated at 30°C until $OD_{600}$ = 0.3. Cell
695 samples were visualized on 1% (w/v) agarose pads by phase contrast microscopy.
696 Bar = 5 μm.

697

698

699

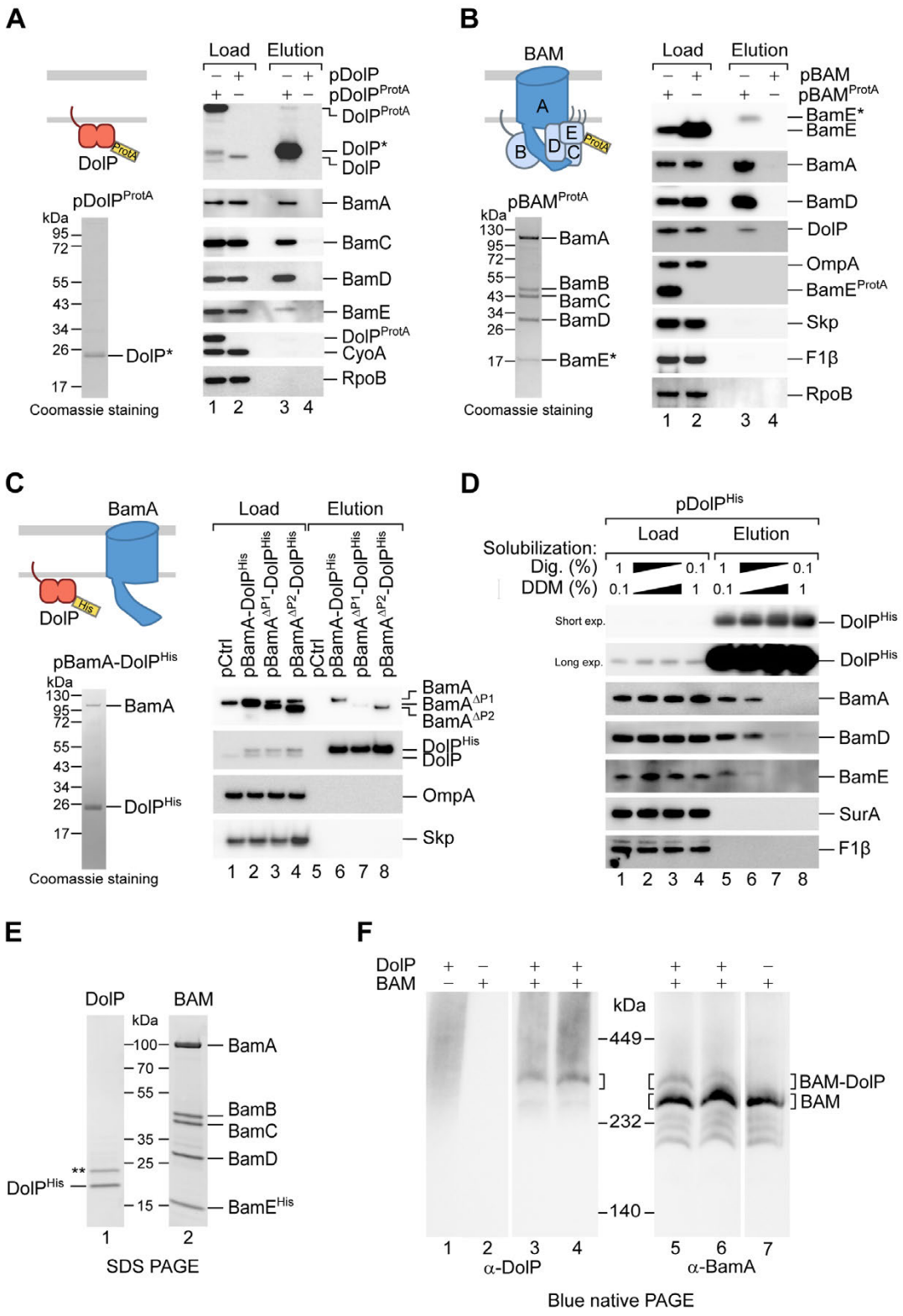
A
Load
Elution
pDolP
pDolP^ProtA
DolP^ProtA
DolP*
DolP
ProtA
DolP
pDolP^ProtA
kDa
95
72
55
43
34
26
17
DolP*
Coomassie staining
BamA
BamC
BamD
BamE
DolP^ProtA
CyoA
RpoB
1 2 3 4
B
BAM
A
B
D
E
C
ProtA
pBAM
pBAM^ProtA
BamE*
BamE
BamA
BamD
DolP
OmpA
BamE^ProtA
Skp
F1β
RpoB
pBAM^ProtA
kDa
130
95
72
55
43
34
26
17
BamA
BamB
BamC
BamD
BamE*
Coomassie staining
1 2 3 4
C
BamA
DolP
His
pBamA-DolP^His
kDa
130
95
72
55
43
34
26
17
BamA
DolP^His
Coomassie staining
Load
Elution
pCtrl
pBamA-DolP^His
pBamA^ΔP1-DolP^His
pBamA^ΔP2-DolP^His
pCtrl
pBamA-DolP^His
pBamA^ΔP1-DolP^His
pBamA^ΔP2-DolP^His
BamA
BamA^ΔP1
BamA^ΔP2
DolP^His
DolP
OmpA
Skp
1 2 3 4 5 6 7 8
D
pDolP^His
Load
Elution
Solubilization:
Dig. (%)
1
0.1
1
0.1
DDM (%)
0.1
1
0.1
1
Short exp.
Long exp.
DolP^His
DolP^His
BamA
BamD
BamE
SurA
F1β
1 2 3 4 5 6 7 8
E
DolP
BAM
kDa
100
70
55
35
25
15
BamA
BamB
BamC
BamD
BamE^His
DolP^His
**
1
2
SDS PAGE
F
DolP
BAM
kDa
449
232
140
BAM-DolP
BAM
1 2 3 4
α-DolP
5 6 7
α-BamA
Blue native PAGE

**Figure 3.**

700

701 **Fig. 3. DolP associates with the BAM complex via an interaction with BamA.**

702 (**A**, **B**). The envelope fraction of BW25113 cells carrying the indicated plasmids
703 were solubilized with 1% (w/v) digitonin and 0.1% (w/v) DDM and subjected to IgG
704 affinity purification of either protein A-tagged DolP (A) or BamE (B). The load and
705 elution fractions were analyzed by SDS-PAGE. The coomassie staining of the
706 elution of protein A-tagged DolP (A) or protein A-tagged BamE (B) are shown below
707 the diagrams representing overproduced proteins. Blotted protein from load and
708 elution fractions were detected by immunodecoration using the indicated antisera.
709 Load 0.5% (A) 1% (B); Elution 100%. The asterisk indicates the products of TEV
710 digestion obtained with samples containing $DolP^{ProtA}$ (A) or $BamE^{ProtA}$ (B).

711 (**C**) The envelope fraction of BW25113 cells carrying the plasmids overproducing
712 His-tagged DolP and the indicated BamA protein variants (deleted of POTRA1 or of
713 POTRA2) were solubilized with 1% (w/v) digitonin and 0.1% (w/v) DDM and
714 subjected to Ni-affinity purification. The load and elution fractions were analyzed by
715 SDS-PAGE. The coomassie staining of the elution of His-tagged DolP
716 overproduced together with wild-type BamA is shown below the diagram
717 representing overproduced proteins. Blotted protein from load and elution fractions
718 were detected by immunodecoration using the indicated antisera. Load 2%; Elution
719 100%.

720 (**D**) Equal aliquots of the envelope fraction of BW25113 cells expressing His-tagged
721 DolP were solubilized with the indicated concentrations of digitonin and DDM
722 (digitonin [w/v], DDM [w/v]): 1%, 0.1% (lane 1), 0.8%, 0.3% (lane 2), 0.3%, 0.8%
723 (lane 3), 0.1%, 1% (lane 4). His-tagged DolP was purified by Ni-affinity
724 chromatography. In all cases, proteins were eluted in the presence of 0.3% (w/v)
725 digitonin and 0.03% (w/v) DDM. Load 0.2%; Elution 100%.

726 (**E**) The envelope fraction of BW25113 cells overproducing $DolP^{His}$ or the BAM
727 complex containing C-terminally His-tagged BamE was subjected to protein
728 extraction with 1% (w/v) DDM and Ni-affinity purification and gel filtration

729 chromatographies. The elution fractions were analyzed by SDS-PAGE and
730 coomassie staining. The double asterisk indicates a contaminant protein in the
731 elution of DolP.

732 (**F**) Purified His-tagged BAM complex and DolP were incubated alone for 1 hour at
733 4°C (lanes 1, 2 and 7), or together for 1 hour at 4°C (lanes 3 and 6) or for 30 min at
734 25°C (lanes 4 and 5), prior to blue native-PAGE and immunoblotting using the
735 indicated antisera.
736

737

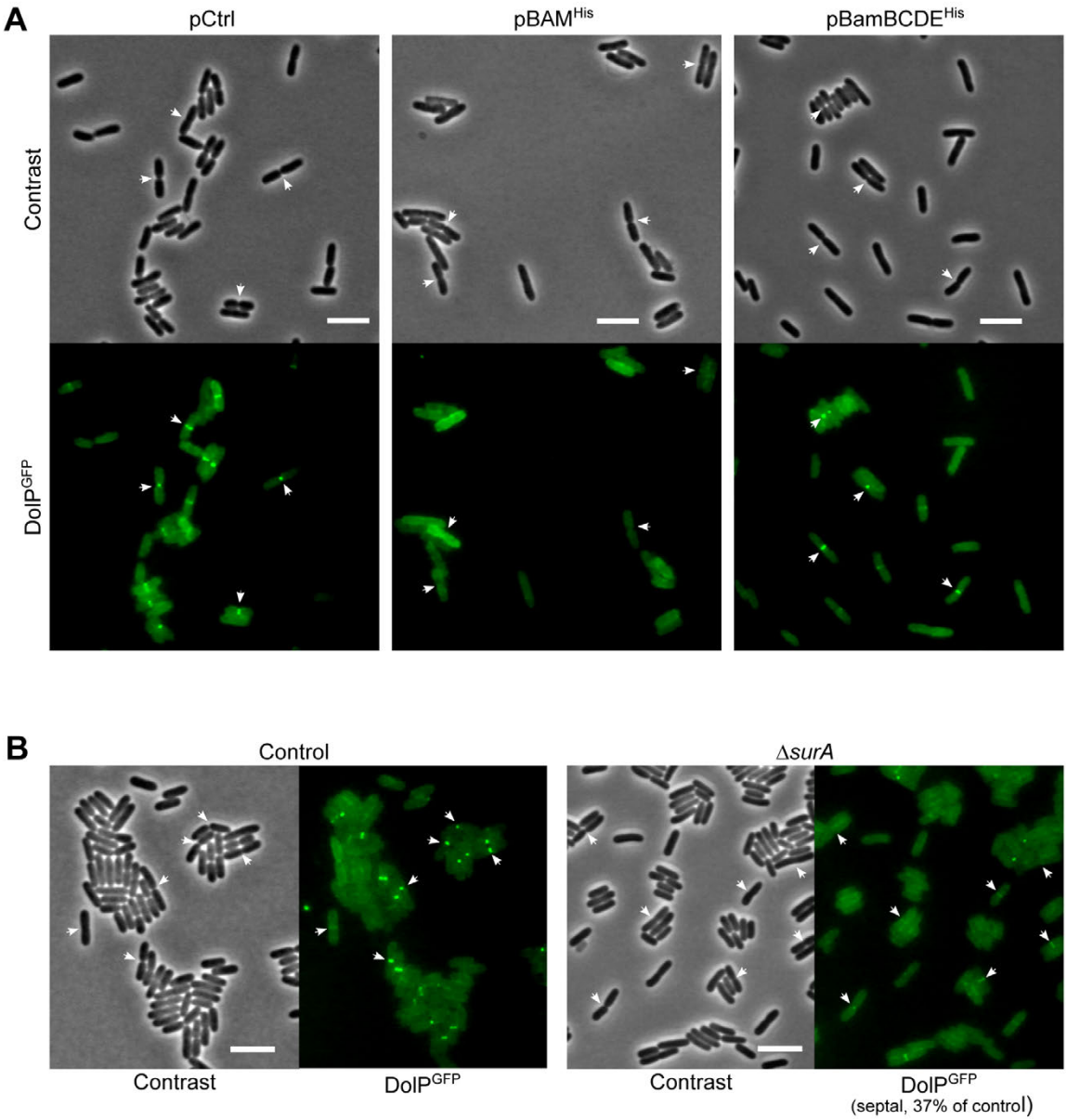


**Figure 4.**

738

739 **Fig. 4. BamA overaccumulation in the OM and envelope stress interfere with**
740 **mid-cell localization of DolP.**

741 (**A**) Overnight cultures of BW25113 cells harboring the chromosomal fusion *dolP-*
742 *gfp* and transformed with either pCtrl (empty vector) or pBAM$^{His}$, or pBamBCDE$^{His}$
743 were freshly diluted in minimal M9 medium, incubated at 30°C until $OD_{600}$ = 0.1 and
744 supplemented with 400 μM IPTG for 1 hour. Cell samples were visualized on 1%
745 (w/v) agarose pads by phase contrast and fluorescence microscopy. Arrowheads
746 indicate envelope constriction sites between forming daughter cells. Bar = 5 μm.

747 (**B**) Overnight cultures of BW25113 (control) or Δ*surA* derivative cells carrying the
748 *dolP-gfp* chromosomal fusion were freshly diluted in LB medium and incubated at
749 30°C until $OD_{600}$ = 0.3. Cell samples were visualized as in (A). Bar = 5 μm. The
750 percentage of cells presenting fluorescent DolP$^{GFP}$ signals at division septa in Δ*surA*
751 cells was normalized to the same fraction obtained for the control cells and reported
752 below the micrograph. More than 1000 cells were counted in each sample.

753

754

755

## References


1 den Blaauwen, T., Hamoen, L. W. & Levin, P. A. The divisome at 25: the road ahead. *Current opinion in microbiology* **36**, 85-94, doi:10.1016/j.mib.2017.01.007 (2017).

2 Egan, A. J. F., Errington, J. & Vollmer, W. Regulation of peptidoglycan synthesis and remodelling. *Nature reviews. Microbiology*, doi:10.1038/s41579-020-0366-3 (2020).

3 Calmettes, C., Judd, A. & Moraes, T. F. Structural Aspects of Bacterial Outer Membrane Protein Assembly. *Advances in experimental medicine and biology* **883**, 255-270, doi:10.1007/978-3-319-23603-2_14 (2015).

4 Nikaido, H. Molecular basis of bacterial outer membrane permeability revisited. *Microbiology and molecular biology reviews : MMBR* **67**, 593-656, doi:10.1128/mmbr.67.4.593-656.2003 (2003).

5 Ranava, D., Caumont-Sarcos, A., Albenne, C. & Ieva, R. Bacterial machineries for the assembly of membrane-embedded beta-barrel proteins. *FEMS microbiology letters* **365**, doi:10.1093/femsle/fny087 (2018).

6 Schiffrin, B., Brockwell, D. J. & Radford, S. E. Outer membrane protein folding from an energy landscape perspective. *BMC biology* **15**, 123, doi:10.1186/s12915-017-0464-5 (2017).

7 Webb, C. T., Heinz, E. & Lithgow, T. Evolution of the beta-barrel assembly machinery. *Trends in microbiology* **20**, 612-620, doi:10.1016/j.tim.2012.08.006 (2012).

8 Voulhoux, R., Bos, M. P., Geurtsen, J., Mols, M. & Tommassen, J. Role of a highly conserved bacterial protein in outer membrane protein assembly. *Science (New York, N.Y.)* **299**, 262-265, doi:10.1126/science.1078973 (2003).

9 Noinaj, N., Kuszak, A. J., Gumbart, J. C., Lukacik, P., Chang, H., Easley, N. C., Lithgow, T. & Buchanan, S. K. Structural insight into the biogenesis of beta-barrel membrane proteins. *Nature* **501**, 385-390, doi:10.1038/nature12521 (2013).

10 Iadanza, M. G., Higgins, A. J., Schiffrin, B., Calabrese, A. N., Brockwell, D. J., Ashcroft, A. E., Radford, S. E. & Ranson, N. A. Lateral opening in the intact beta-barrel assembly machinery captured by cryo-EM. *Nature communications* **7**, 12865, doi:10.1038/ncomms12865 (2016).

11 Gu, Y., Li, H., Dong, H., Zeng, Y., Zhang, Z., Paterson, N. G., Stansfeld, P. J., Wang, Z., Zhang, Y., Wang, W. & Dong, C. Structural basis of outer membrane protein insertion by the BAM complex. *Nature* **531**, 64-69, doi:10.1038/nature17199 (2016).

12 Bakelar, J., Buchanan, S. K. & Noinaj, N. The structure of the beta-barrel assembly machinery complex. *Science (New York, N.Y.)* **351**, 180-186, doi:10.1126/science.aad3460 (2016).

13 Doerner, P. A. & Sousa, M. C. Extreme Dynamics in the BamA beta-Barrel Seam. *Biochemistry* **56**, 3142-3149, doi:10.1021/acs.biochem.7b00281 (2017).

14 Gessmann, D., Chung, Y. H., Danoff, E. J., Plummer, A. M., Sandlin, C. W., Zaccai, N. R. & Fleming, K. G. Outer membrane beta-barrel protein folding is physically controlled by periplasmic lipid head groups and BamA. *Proceedings of the National Academy of Sciences of the United States of America* **111**, 5878-5883, doi:10.1073/pnas.1322473111 (2014).

15 Doyle, M. T. & Bernstein, H. D. Bacterial outer membrane proteins assemble via asymmetric interactions with the BamA beta-barrel. *Nature communications* **10**, 3358, doi:10.1038/s41467-019-11230-9 (2019).

16 Tomasek, D., Rawson, S., Lee, J., Wzorek, J. S., Harrison, S. C., Li, Z. & Kahne, D. Structure of a nascent membrane protein as it folds on the BAM complex. *Nature*, doi:10.1038/s41586-020-2370-1 (2020).

17 Sklar, J. G., Wu, T., Gronenberg, L. S., Malinverni, J. C., Kahne, D. & Silhavy, T. J. Lipoprotein SmpA is a component of the YaeT complex that assembles outer membrane proteins in Escherichia coli. *Proceedings of the National Academy of Sciences of the United States of America* **104**, 6400-6405, doi:10.1073/pnas.0701579104 (2007).

18 Kim, S., Malinverni, J. C., Sliz, P., Silhavy, T. J., Harrison, S. C. & Kahne, D. Structure and function of an essential component of the outer membrane protein assembly machine. *Science (New York, N.Y.)* **317**, 961-964, doi:10.1126/science.1143993 (2007).

19 Wu, T., Malinverni, J., Ruiz, N., Kim, S., Silhavy, T. J. & Kahne, D. Identification of a multicomponent complex required for outer membrane biogenesis in Escherichia coli. *Cell* **121**, 235-245, doi:10.1016/j.cell.2005.02.015 (2005).

20 Bennion, D., Charlson, E. S., Coon, E. & Misra, R. Dissection of beta-barrel outer membrane protein assembly pathways through characterizing BamA POTRA 1 mutants of Escherichia coli. *Molecular microbiology* **77**, 1153-1171, doi:10.1111/j.1365-2958.2010.07280.x (2010).

21 Rizzitello, A. E., Harper, J. R. & Silhavy, T. J. Genetic evidence for parallel pathways of chaperone activity in the periplasm of Escherichia coli. *Journal of bacteriology* **183**, 6794-6800, doi:10.1128/jb.183.23.6794-6800.2001 (2001).

22 Crane, J. M. & Randall, L. L. The Sec System: Protein Export in Escherichia coli. *EcoSal Plus* **7**, doi:10.1128/ecosalplus.ESP-0002-2017 (2017).

23 Walsh, N. P., Alba, B. M., Bose, B., Gross, C. A. & Sauer, R. T. OMP peptide signals initiate the envelope-stress response by activating DegS protease via relief of inhibition mediated by its PDZ domain. *Cell* **113**, 61-71, doi:10.1016/s0092-8674(03)00203-4 (2003).

24 Ades, S. E. Regulation by destruction: design of the sigmaE envelope stress response. *Current opinion in microbiology* **11**, 535-540, doi:10.1016/j.mib.2008.10.004 (2008).

25 Rhodius, V. A., Suh, W. C., Nonaka, G., West, J. & Gross, C. A. Conserved and variable functions of the sigmaE stress response in related genomes. *PLoS biology* **4**, e2, doi:10.1371/journal.pbio.0040002 (2006).

26 Guillier, M., Gottesman, S. & Storz, G. Modulating the outer membrane with small RNAs. *Genes & development* **20**, 2338-2348, doi:10.1101/gad.1457506 (2006).

27 De Las Penas, A., Connolly, L. & Gross, C. A. SigmaE is an essential sigma factor in Escherichia coli. *Journal of bacteriology* **179**, 6862-6864, doi:10.1128/jb.179.21.6862-6864.1997 (1997).

28 Missiakas, D., Mayer, M. P., Lemaire, M., Georgopoulos, C. & Raina, S. Modulation of the Escherichia coli sigmaE (RpoE) heat-shock transcription-factor activity by the RseA, RseB and RseC proteins. *Molecular microbiology* **24**, 355-371, doi:10.1046/j.1365-2958.1997.3601713.x (1997).

854 29 De Las Penas, A., Connolly, L. & Gross, C. A. The sigmaE-mediated
855 response to extracytoplasmic stress in Escherichia coli is transduced by
856 RseA and RseB, two negative regulators of sigmaE. *Molecular microbiology*
857 **24**, 373-385, doi:10.1046/j.1365-2958.1997.3611718.x (1997).
858 30 Nicoloff, H., Gopalkrishnan, S. & Ades, S. E. Appropriate Regulation of the
859 sigma(E)-Dependent Envelope Stress Response Is Necessary To Maintain
860 Cell Envelope Integrity and Stationary-Phase Survival in Escherichia coli.
861 *Journal of bacteriology* **199**, doi:10.1128/jb.00089-17 (2017).
862 31 Mitchell, A. M. & Silhavy, T. J. Envelope stress responses: balancing
863 damage repair and toxicity. *Nature reviews. Microbiology* **17**, 417-428,
864 doi:10.1038/s41579-019-0199-0 (2019).
865 32 Morris, F. C., Wells, T. J., Bryant, J. A., Schager, A. E., Sevastsyanovich, Y.
866 R., Squire, D. J. P., Marshall, J., Isom, G. L., Rooke, J., Maderbocus, R.,
867 Knowles, T. J., Overduin, M., Rossiter, A. E., Cunningham, A. F. &
868 Henderson, I. R. YraP Contributes to Cell Envelope Integrity and Virulence of
869 Salmonella enterica Serovar Typhimurium. *Infection and immunity* **86**,
870 doi:10.1128/iai.00829-17 (2018).
871 33 Tsang, M. J., Yakhnina, A. A. & Bernhardt, T. G. NlpD links cell wall
872 remodeling and outer membrane invagination during cytokinesis in
873 Escherichia coli. *PLoS genetics* **13**, e1006888,
874 doi:10.1371/journal.pgen.1006888 (2017).
875 34 Onufryk, C., Crouch, M. L., Fang, F. C. & Gross, C. A. Characterization of six
876 lipoproteins in the sigmaE regulon. *Journal of bacteriology* **187**, 4552-4561,
877 doi:10.1128/jb.187.13.4552-4561.2005 (2005).
878 35 Seib, K. L., Haag, A. F., Oriente, F., Fantappie, L., Borghi, S., Semchenko, E.
879 A., Schulz, B. L., Ferlicca, F., Taddei, A. R., Giuliani, M. M., Pizza, M. &
880 Delany, I. The meningococcal vaccine antigen GNA2091 is an analogue of
881 YraP and plays key roles in outer membrane stability and virulence. *FASEB*
882 *journal : official publication of the Federation of American Societies for*
883 *Experimental Biology* **33**, 12324-12335, doi:10.1096/fj.201900669R (2019).
884 36 Bos, M. P., Grijpstra, J., Tommassen-van Boxtel, R. & Tommassen, J.
885 Involvement of Neisseria meningitidis lipoprotein GNA2091 in the assembly
886 of a subset of outer membrane proteins. *The Journal of biological chemistry*
887 **289**, 15602-15610, doi:10.1074/jbc.M113.539510 (2014).
888 37 Baba, T., Ara, T., Hasegawa, M., Takai, Y., Okumura, Y., Baba, M.,
889 Datsenko, K. A., Tomita, M., Wanner, B. L. & Mori, H. Construction of
890 Escherichia coli K-12 in-frame, single-gene knockout mutants: the Keio
891 collection. *Molecular systems biology* **2**, 2006.0008,
892 doi:10.1038/msb4100050 (2006).
893 38 Cui, L., Vigouroux, A., Rousset, F., Varet, H., Khanna, V. & Bikard, D. A
894 CRISPRi screen in E. coli reveals sequence-specific toxicity of dCas9.
895 *Nature communications* **9**, 1912, doi:10.1038/s41467-018-04209-5 (2018).
896 39 Calvo-Villamanan, A., Ng, J. W., Planel, R., Menager, H., Chen, A., Cui, L. &
897 Bikard, D. On-target activity predictions enable improved CRISPR-dCas9
898 screens in bacteria. *Nucleic acids research*, doi:10.1093/nar/gkaa294 (2020).
899 40 Pichoff, S., Du, S. & Lutkenhaus, J. Roles of FtsEX in cell division. *Research*
900 *in microbiology* **170**, 374-380, doi:10.1016/j.resmic.2019.07.003 (2019).
901 41 Heidrich, C., Templin, M. F., Ursinus, A., Merdanovic, M., Berger, J.,
902 Schwarz, H., de Pedro, M. A. & Holtje, J. V. Involvement of N-acetylmuramyl-
903 L-alanine amidases in cell separation and antibiotic-induced autolysis of

904 Escherichia coli. *Molecular microbiology* **41**, 167-178, doi:10.1046/j.1365-
905 2958.2001.02499.x (2001).
906 42 Uehara, T., Dinh, T. & Bernhardt, T. G. LytM-domain factors are required for
907 daughter cell separation and rapid ampicillin-induced lysis in Escherichia coli.
908 *Journal of bacteriology* **191**, 5094-5107, doi:10.1128/jb.00505-09 (2009).
909 43 Yang, D. C., Peters, N. T., Parzych, K. R., Uehara, T., Markovski, M. &
910 Bernhardt, T. G. An ATP-binding cassette transporter-like complex governs
911 cell-wall hydrolysis at the bacterial cytokinetic ring. *Proceedings of the*
912 *National Academy of Sciences of the United States of America* **108**, E1052-
913 1060, doi:10.1073/pnas.1107780108 (2011).
914 44 Uehara, T., Parzych, K. R., Dinh, T. & Bernhardt, T. G. Daughter cell
915 separation is controlled by cytokinetic ring-activated cell wall hydrolysis. *The*
916 *EMBO journal* **29**, 1412-1422, doi:10.1038/emboj.2010.36 (2010).
917 45 Chung, H. S., Yao, Z., Goehring, N. W., Kishony, R., Beckwith, J. & Kahne,
918 D. Rapid beta-lactam-induced lysis requires successful assembly of the cell
919 division machinery. *Proceedings of the National Academy of Sciences of the*
920 *United States of America* **106**, 21872-21877, doi:10.1073/pnas.0911674106
921 (2009).
922 46 Malinverni, J. C., Werner, J., Kim, S., Sklar, J. G., Kahne, D., Misra, R. &
923 Silhavy, T. J. YfiO stabilizes the YaeT complex and is essential for outer
924 membrane protein assembly in Escherichia coli. *Molecular microbiology* **61**,
925 151-164, doi:10.1111/j.1365-2958.2006.05211.x (2006).
926 47 Carlson, M. L., Stacey, R. G., Young, J. W., Wason, I. S., Zhao, Z., Rattray,
927 D. G., Scott, N., Kerr, C. H., Babu, M., Foster, L. J. & Duong Van Hoa, F.
928 Profiling the Escherichia coli membrane protein interactome captured in
929 Peptidisc libraries. *eLife* **8**, doi:10.7554/eLife.46615 (2019).
930 48 Alvira, S., Watkins, D. W., Troman, L., Allen, W. J., Lorriman, J.,
931 Degliesposti, G., Cohen, E. J., Beeby, M., Daum, B., Gold, V. A. M., Skehel,
932 J. M. & Collinson, I. Inter-membrane association of the Sec and BAM
933 translocons for bacterial outer-membrane biogenesis. *bioRxiv*, 589077,
934 doi:10.1101/589077 (2020).
935 49 Rouviere, P. E. & Gross, C. A. SurA, a periplasmic protein with peptidyl-prolyl
936 isomerase activity, participates in the assembly of outer membrane porins.
937 *Genes & development* **10**, 3170-3182, doi:10.1101/gad.10.24.3170 (1996).
938 50 McBroom, A. J. & Kuehn, M. J. Release of outer membrane vesicles by
939 Gram-negative bacteria is a novel envelope stress response. *Molecular*
940 *microbiology* **63**, 545-558, doi:10.1111/j.1365-2958.2006.05522.x (2007).
941 51 Roman-Hernandez, G., Peterson, J. H. & Bernstein, H. D. Reconstitution of
942 bacterial autotransporter assembly using purified components. *eLife* **3**,
943 e04234, doi:10.7554/eLife.04234 (2014).
944 52 Hale, C. A. & de Boer, P. A. Direct binding of FtsZ to ZipA, an essential
945 component of the septal ring structure that mediates cell division in E. coli.
946 *Cell* **88**, 175-185, doi:10.1016/s0092-8674(00)81838-3 (1997).
947 53 Hartmann, J. B., Zahn, M., Burmann, I. M., Bibow, S. & Hiller, S. Sequence-
948 Specific Solution NMR Assignments of the beta-Barrel Insertase BamA to
949 Monitor Its Conformational Ensemble at the Atomic Level. *Journal of the*
950 *American Chemical Society* **140**, 11252-11260, doi:10.1021/jacs.8b03220
951 (2018).
952 54 Vertommen, D., Ruiz, N., Leverrier, P., Silhavy, T. J. & Collet, J. F.
953 Characterization of the role of the Escherichia coli periplasmic chaperone

954 SurA using differential proteomics. *Proteomics* **9**, 2432-2443,
955 doi:10.1002/pmic.200800794 (2009).
956 55 Konovalova, A., Schwalm, J. A. & Silhavy, T. J. A Suppressor Mutation That
957 Creates a Faster and More Robust sigmaE Envelope Stress Response.
958 *Journal of bacteriology* **198**, 2345-2351, doi:10.1128/jb.00340-16 (2016).
959 56 Kern, B., Leiser, O. P. & Misra, R. Suppressor Mutations in degS Overcome
960 the Acute Temperature-Sensitive Phenotype of DeltadegP and DeltadegP
961 Deltatol-pal Mutants of Escherichia coli. *Journal of bacteriology* **201**,
962 doi:10.1128/jb.00742-18 (2019).
963 57 Hart, E. M., O'Connell, A., Tang, K., Wzorek, J. S., Grabowicz, M., Kahne, D.
964 & Silhavy, T. J. Fine-Tuning of sigma(E) Activation Suppresses Multiple
965 Assembly-Defective Mutations in Escherichia coli. *Journal of bacteriology*
966 **201**, doi:10.1128/jb.00745-18 (2019).
967 58 Leiser, O. P., Charlson, E. S., Gerken, H. & Misra, R. Reversal of the ΔdegP
968 phenotypes by a novel rpoE allele of Escherichia coli. *PloS one* **7**, e33979,
969 doi:10.1371/journal.pone.0033979 (2012).
970 59 Yeats, C. & Bateman, A. The BON domain: a putative membrane-binding
971 domain. *Trends in biochemical sciences* **28**, 352-355, doi:10.1016/s0968-
972 0004(03)00115-4 (2003).
973 60 Bryant, J. A., Morris, F. C., Knowles, T. J., Maderbocus, R., Heinz, E.,
974 Boelter, G., Alodaini, D., Colyer, A., Wotherspoon, P. J., Staunton, K. A.,
975 Jeeves, M., Browning, D. F., Sevastsyanovich, Y. R., Wells, T. J., Rossiter,
976 A. E., Bavro, V. N., Sridhar, P., Ward, D. G., Chong, Z. S., Icke, C., Teo, A.,
977 Chng, S. S., Roper, D. I., Lithgow, T., Cunningham, A. F., Banzhaf, M.,
978 Overduin, M. & Henderson, I. R. Structure-function analyses of dual-BON
979 domain protein DolP identifies phospholipid binding as a new mechanism for
980 protein localisation. *bioRxiv*, 2020.2008.2010.244616,
981 doi:10.1101/2020.08.10.244616 (2020).
982 61 Fleming, K. G. A combined kinetic push and thermodynamic pull as driving
983 forces for outer membrane protein sorting and folding in bacteria.
984 *Philosophical transactions of the Royal Society of London. Series B,*
985 *Biological sciences* **370**, doi:10.1098/rstb.2015.0026 (2015).
986 62 Horne, J. E., Brockwell, D. J. & Radford, S. E. Role of the lipid bilayer in
987 outer membrane protein folding in Gram-negative bacteria. *The Journal of*
988 *biological chemistry* **295**, 10340-10367, doi:10.1074/jbc.REV120.011473
989 (2020).
990 63 Sinnige, T., Weingarth, M., Renault, M., Baker, L., Tommassen, J. & Baldus,
991 M. Solid-state NMR studies of full-length BamA in lipid bilayers suggest
992 limited overall POTRA mobility. *Journal of molecular biology* **426**, 2009-2021,
993 doi:10.1016/j.jmb.2014.02.007 (2014).
994 64 Rassam, P., Copeland, N. A., Birkholz, O., Tóth, C., Chavent, M., Duncan, A.
995 L., Cross, S. J., Housden, N. G., Kaminska, R., Seger, U., Quinn, D. M.,
996 Garrod, T. J., Sansom, M. S., Piehler, J., Baumann, C. G. & Kleanthous, C.
997 Supramolecular assemblies underpin turnover of outer membrane proteins in
998 bacteria. *Nature* **523**, 333-336, doi:10.1038/nature14461 (2015).
999 65 Gunasinghe, S. D., Shiota, T., Stubenrauch, C. J., Schulze, K. E., Webb, C.
1000 T., Fulcher, A. J., Dunstan, R. A., Hay, I. D., Naderer, T., Whelan, D. R., Bell,
1001 T. D. M., Elgass, K. D., Strugnell, R. A. & Lithgow, T. The WD40 Protein
1002 BamB Mediates Coupling of BAM Complexes into Assembly Precincts in the

Bacterial Outer Membrane. *Cell reports* **23**, 2782-2794, doi:10.1016/j.celrep.2018.04.093 (2018).

66 Jarosławski, S., Duquesne, K., Sturgis, J. N. & Scheuring, S. High-resolution architecture of the outer membrane of the Gram-negative bacteria Roseobacter denitrificans. *Molecular microbiology* **74**, 1211-1222, doi:10.1111/j.1365-2958.2009.06926.x (2009).

67 Lessen, H. J., Fleming, P. J., Fleming, K. G. & Sodt, A. J. Building Blocks of the Outer Membrane: Calculating a General Elastic Energy Model for β-Barrel Membrane Proteins. *Journal of chemical theory and computation* **14**, 4487-4497, doi:10.1021/acs.jctc.8b00377 (2018).

68 Choi, U. & Lee, C. R. Distinct Roles of Outer Membrane Porins in Antibiotic Resistance and Membrane Integrity in Escherichia coli. *Frontiers in microbiology* **10**, 953, doi:10.3389/fmicb.2019.00953 (2019).

69 Delhaye, A., Collet, J. F. & Laloux, G. A Fly on the Wall: How Stress Response Systems Can Sense and Respond to Damage to Peptidoglycan. *Frontiers in cellular and infection microbiology* **9**, 380, doi:10.3389/fcimb.2019.00380 (2019).

70 Macritchie, D. M. & Raivio, T. L. Envelope Stress Responses. *EcoSal Plus* **3**, doi:10.1128/ecosalplus.5.4.7 (2009).

71 Grabowicz, M. & Silhavy, T. J. Envelope Stress Responses: An Interconnected Safety Net. *Trends in biochemical sciences* **42**, 232-242, doi:10.1016/j.tibs.2016.10.002 (2017).

72 Grenier, F., Matteau, D., Baby, V. & Rodrigue, S. Complete Genome Sequence of Escherichia coli BW25113. *Genome announcements* **2**, doi:10.1128/genomeA.01038-14 (2014).

73 Blattner, F. R., Plunkett, G., 3rd, Bloch, C. A., Perna, N. T., Burland, V., Riley, M., Collado-Vides, J., Glasner, J. D., Rode, C. K., Mayhew, G. F., Gregor, J., Davis, N. W., Kirkpatrick, H. A., Goeden, M. A., Rose, D. J., Mau, B. & Shao, Y. The complete genome sequence of Escherichia coli K-12. *Science (New York, N.Y.)* **277**, 1453-1462, doi:10.1126/science.277.5331.1453 (1997).

74 Datsenko, K. A. & Wanner, B. L. One-step inactivation of chromosomal genes in Escherichia coli K-12 using PCR products. *Proceedings of the National Academy of Sciences of the United States of America* **97**, 6640-6645, doi:10.1073/pnas.120163297 (2000).

75 Knop, M., Siegers, K., Pereira, G., Zachariae, W., Winsor, B., Nasmyth, K. & Schiebel, E. Epitope tagging of yeast genes using a PCR-based strategy: more tags and improved practical routines. *Yeast (Chichester, England)* **15**, 963-972, doi:10.1002/(sici)1097-0061(199907)15:10b<963::Aid-yea399>3.0.Co;2-w (1999).

76 McLeay, R. C. & Bailey, T. L. Motif Enrichment Analysis: a unified framework and an evaluation on ChIP data. *BMC bioinformatics* **11**, 165, doi:10.1186/1471-2105-11-165 (2010).

77 Ieva, R. & Bernstein, H. D. Interaction of an autotransporter passenger domain with BamA during its translocation across the bacterial outer membrane. *Proceedings of the National Academy of Sciences of the United States of America* **106**, 19120-19125, doi:10.1073/pnas.0907912106 (2009).

**Supplementary Materials**

# Outer membrane lipoprotein DolP interacts with the BAM complex and promotes fitness during envelope stress response

David Ranava, Yiying Yang, Luis Orenday-Tapia, François Rousset, Catherine Turlan, Lun Cui, Violette Morales, Cyril Moulin, Gladys Munoz, Jérôme Rech, Anne Caumont-Sarcos, Cécile Albenne, David Bikard, Raffaele Ieva

10

11

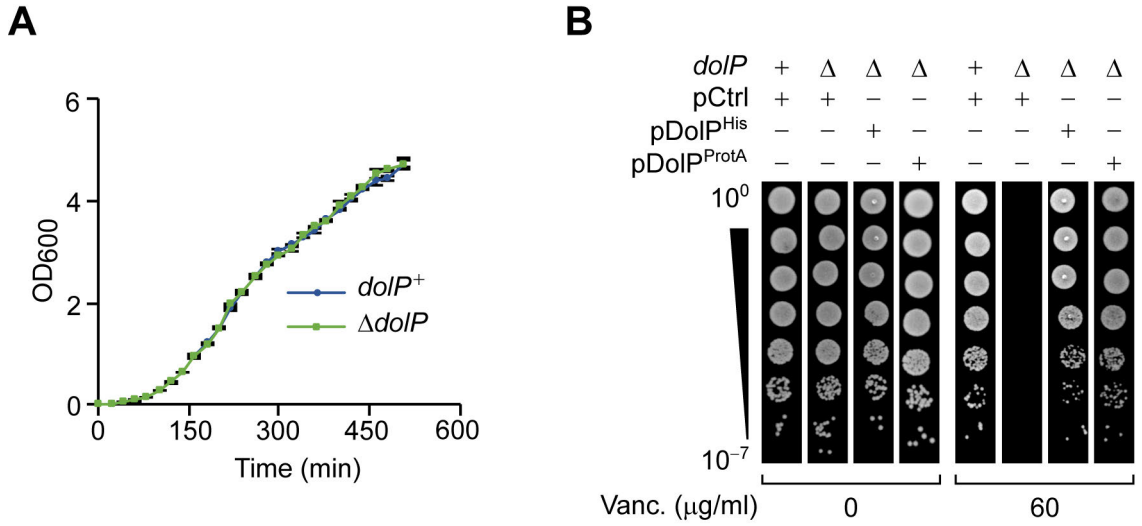


# Figure S1.

12
13 **Fig. S1. The deletion of *dolP* severely impairs growth in the presence of**
14 **vancomycin.**

15 (**A**) BW25113 and Δ*dolP* cells were cultured in LB. The cell densities of both cultures
16 were monitored by measuring the $OD_{600}$ at regular time intervals. The graph reports
17 mean values of independent cultures ± standard deviation (SD, *n* = 3).

18 (**B**) BW25113 and Δ*dolP* cells carrying the indicated plasmids were serially diluted
19 and spotted on LB containing 60 μg/ml vancomycin where indicated. Ectopic
20 expression was driven by the leaky transcriptional activity of $P_{trc}$ in the absence of
21 IPTG.

22

23

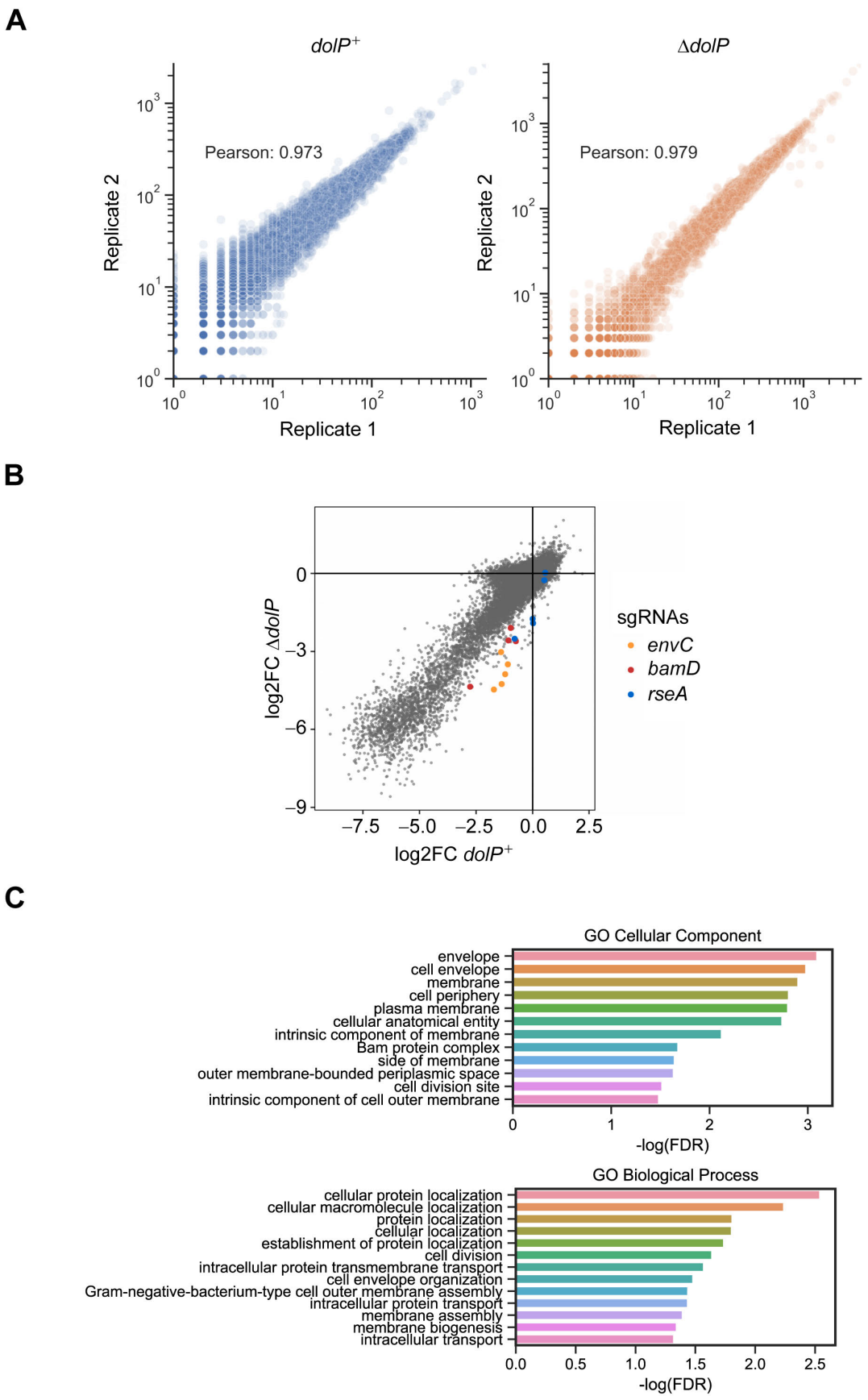
A
dolP+
ΔdolP
Pearson: 0.973
Pearson: 0.979
Replicate 2
Replicate 1
B
log2FC ΔdolP
log2FC dolP+
sgRNAs
envC
bamD
rseA
C
GO Cellular Component
envelope
cell envelope
membrane
cell periphery
plasma membrane
cellular anatomical entity
intrinsic component of membrane
Bam protein complex
side of membrane
outer membrane-bounded periplasmic space
cell division site
intrinsic component of cell outer membrane
-log(FDR)
GO Biological Process
cellular protein localization
cellular macromolecule localization
protein localization
cellular localization
establishment of protein localization
cell division
intracellular protein transmembrane transport
cell envelope organization
Gram-negative-bacterium-type cell outer membrane assembly
intracellular protein transport
membrane assembly
membrane biogenesis
intracellular transport
-log(FDR)

**Figure S2.**

24

25

26 **Fig. S2. Reproducibility of the CRISPRi screens and ontology analysis of gene**
27 **hits.**

28 (**A**) The raw read counts of experimental replicates are very well correlated
29 (Pearson's r > 0.97) in both *dolP*$^{+}$ (left) and Δ*dolP* (right) screens.

30 (**B**) Log2FC values of each sgRNA are compared between the WT and Δ*dolP*
31 screens. Only guides targeting *envC*, *bamD*, and *rseA* are highlighted in orange, red
32 and cyan, respectively.

33 (**C**) Gene Ontology analysis of the genes with a significant synthetic interaction with
34 *dolP*. Using FDR<0.05 as a threshold, 27 genes were selected for Gene Ontology
35 (GO) analysis for cellular component (upper panel) or biological process (bottom
36 panel)[78]. Both analyses show an overrepresentation of genes associated with cell
37 envelope and membrane function.

38

39

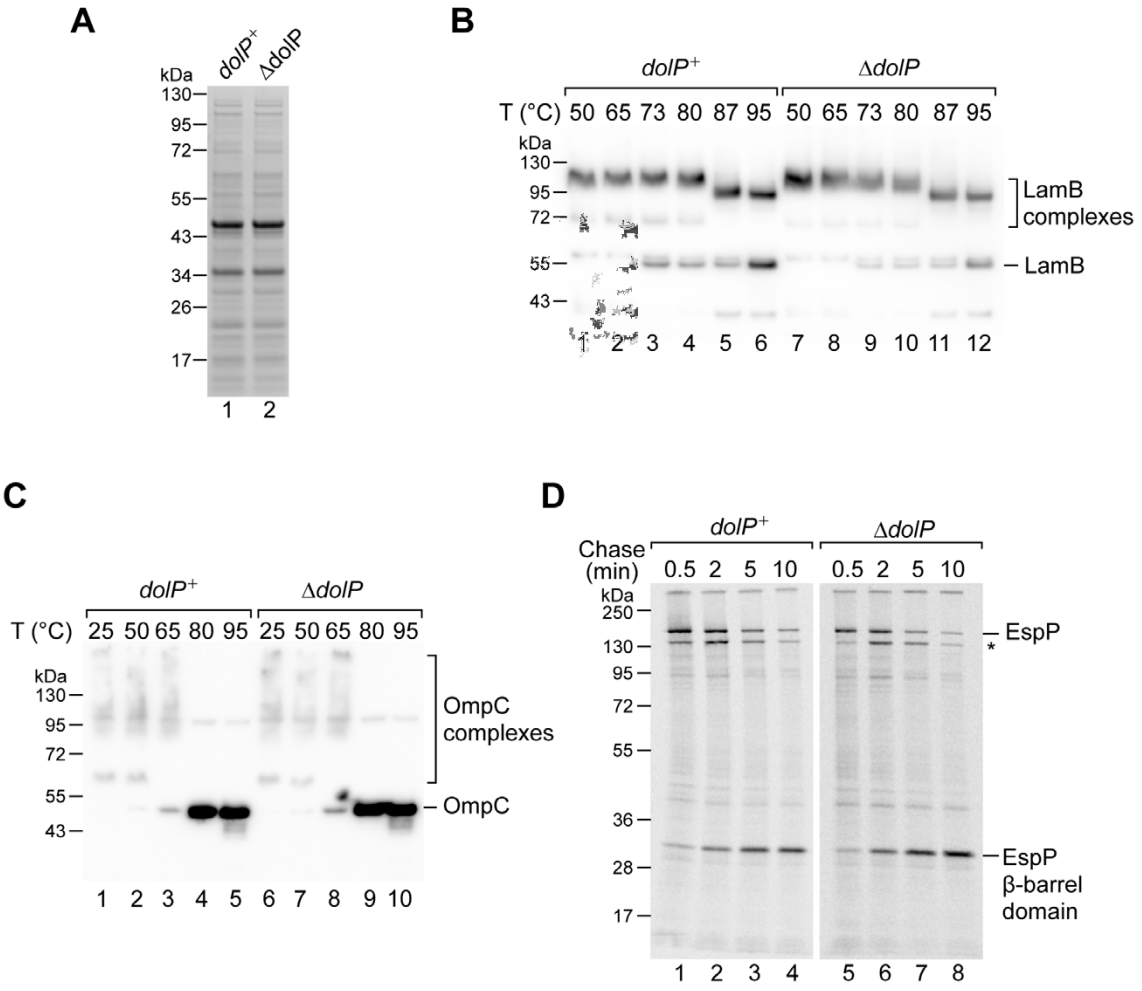


**Figure S3.**

40
41

42

43 **Fig. S3. DolP is not crucial for OMP biogenesis.**

44 (**A**) The protein content of the envelope fraction of BW25113 (*dolP*$^+$) or Δ*dolP* cells
45 was mixed with SDS-PAGE loading buffer and analyzed by SDS-PAGE and
46 coomassie staining.

47 (**B** and **C**) The protein content of the envelope fraction of BW25113 (*dolP*$^+$) and
48 Δ*dolP* cells was mixed with SDS-PAGE loading buffer, heated at the indicated
49 temperatures, separated by SDS-PAGE and immunoblotted using anti-LamB (B) or
50 anti-OmpC (C) antisera. LamB and OmpC form complexes (trimers), which are
51 resistant to SDS and require significant heating to be denatured. At progressively
52 higher temperatures, LamB (B) and OmpC (C) complexes are denatured and the two
53 proteins migrate as monomers. The amounts of LamB and OmpC complexes or
54 denatured monomers and the temperature-dependent patterns of complex-to-
55 monomer conversion do not appear to depend on *dolP* expression.

56 (**D**) The biogenesis of EspP, an autotransporter OMP of enterohemorrhagic *E. coli*
57 heterologously expressed in BW25113 cells, was monitored in time. The plasmid
58 pRI22[79] harbouring the EspP encoding gene under the control of an IPTG-inducible
59 promoter was transformed into wild-type BW25113 (*dolP*$^+$) and Δ*dolP* cells. EspP is a
60 serine protease autotransporter of *Enterobacteriaceae*, and consists of an N-terminal
61 passenger domain secreted on the cell surface and a C-terminal domain which is
62 ultimately folded into an integral OM β-barrel structure[80]. EspP biogenesis requires
63 both periplasmic chaperones, such as SurA, and the BAM complex[79]. Once EspP
64 assembly and secretion are completed, the passenger domain is cleaved by an
65 autocatalytic reaction that is catalyzed by residues of the folded β-barrel domain
66 facing the interior of the barrel. Thus, the proteolytic reaction can be exploited to infer
67 about completion of β-barrel folding and assembly[80,81]. To monitor the kinetics of
68 EspP autoproteolysis, cells carrying pRI22 were cultured in M9 minimal medium until
69 early exponential phase, supplemented with 200 μM IPTG and subjected to $^{35}$S

70 pulse-chase labelling. The total protein contents of samples collected after the
71 indicated chase times were subjected to immunoprecipitation using an antiserum
72 specific for an EspP C-terminal peptide. The asterisk indicates a degradation product
73 of EspP, likely generated by the OM protease OmpT, which cleaves the N-terminal
74 region of the passenger domain as it is secreted across the OM[82]. A band
75 corresponding to the EspP β-barrel domain is generated with a similar time
76 dependence in both *dolP*$^{+}$ and Δ*dolP* cells.
77
78

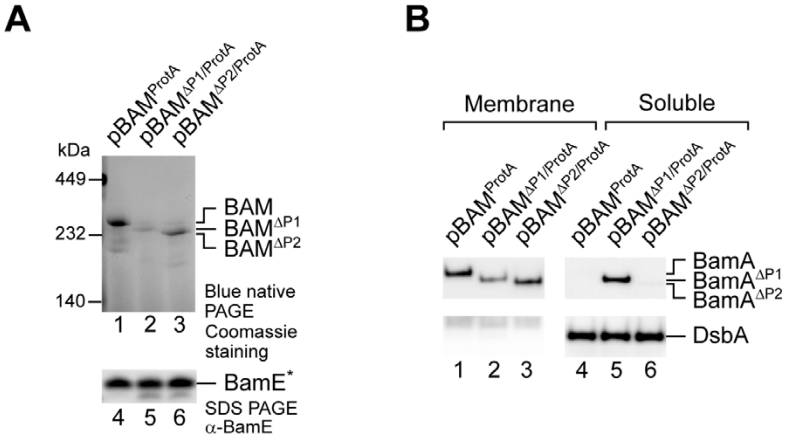
A
pBAM^ProtA
pBAM^ΔP1/ProtA
pBAM^ΔP2/ProtA
kDa
449
232
140
BAM
BAM^ΔP1
BAM^ΔP2
Blue native PAGE
Coomassie staining
1 2 3
BamE*
SDS PAGE
α-BamE
4 5 6
B
Membrane
Soluble
pBAM^ProtA
pBAM^ΔP1/ProtA
pBAM^ΔP2/ProtA
pBAM^ProtA
pBAM^ΔP1/ProtA
pBAM^ΔP2/ProtA
BamA
BamA^ΔP1
BamA^ΔP2
DsbA
1 2 3 4 5 6

**Figure S4.**

81 **Fig. S4. Overproduced BAM accumulates in the OM**

82 (**A**) The crude envelope fractions of cells overproducing $BAM^{ProtA}$, $BAM^{\Delta P1/ProtA}$, or
83 $BAM^{\Delta P2/ProtA}$ were solubilized with 1% (w/v) digitonin and 0.1% (w/v) DDM and
84 subjected to native IgG-affinity chromatography. Elutions were analyzed by blue
85 native-PAGE and coomassie staining (lanes 1-3) or SDS-PAGE and immunoblotting
86 (lanes 4-6). Blue native-PAGE of the elution fraction containing wild-type BamA
87 resolved a coomassie stainable complex migrating with an apparent mass of 250
88 kDa, which corresponds to the BAM complex (lane 1). A roughly similar amount of
89 BAM complex was detected in the elution obtained with $BamA^{\Delta P2/ProtA}$ samples,
90 although in this case the $BAM^{\Delta P2}$ complex migrated slightly faster, accounting for the
91 $BamA^{\Delta P2}$ mass difference (lane 3). In contrast, the amount of $BAM^{\Delta P1/ProtA}$ variant was
92 considerably lower (lane 2). The asterisk indicates that BamE is obtained from TEV
93 digestion of $BamE^{ProtA}$.

94 (**B**) Cells overproducing the indicated variants of the BAM complex were fractionated.
95 The membrane and soluble fractions, obtained upon treatment of collected cells with
96 lysozyme and EDTA were analyzed by SDS-PAGE and immunoblotting. $BamA^{\Delta P1}$
97 was depleted from the total membrane fraction (lanes 1-3), and accumulated in the
98 soluble fraction containing the periplasmic protein DsbA (lanes 4-6).
99

100

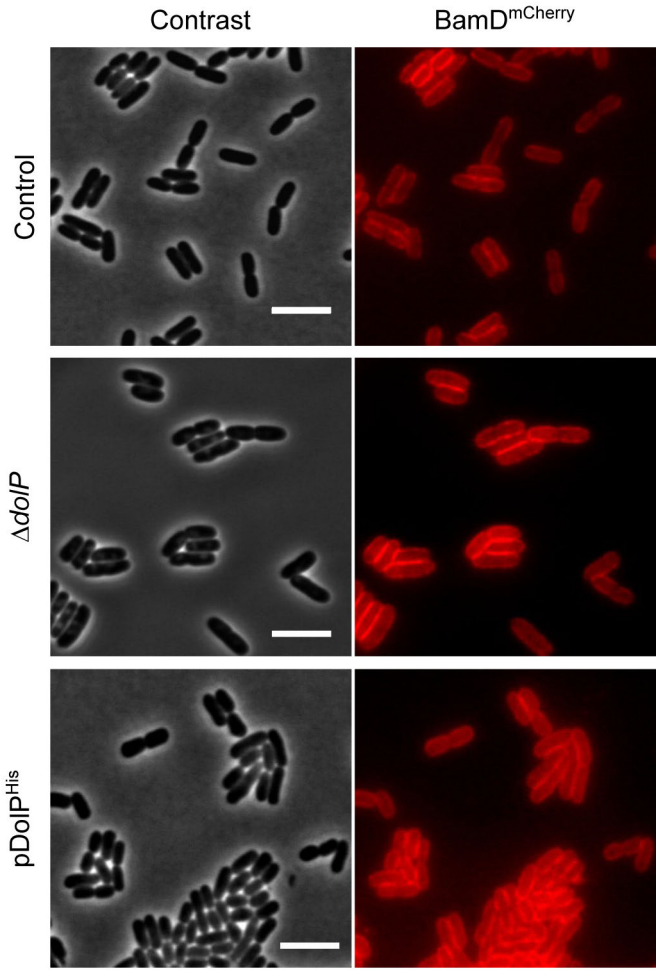


**Figure S5.**

101

102 **Fig. S5. Effect of lack or overproduction of DolP on BAM localization.**

103 BW25113 derivative cells harbouring a *bamD-mCherry* chromosomal fusion were
104 visualized on 1% (w/v) agarose pads by fluorescence and phase-contrast
105 microscopy. Top: *dolP*$^{+}$ cells (control); Center: Δ*dolP* cells: Bottom: *dolP*$^{+}$ cells
106 carrying pDolP$^{His}$. Cells were cultured at 30°C in minimal M9 medium to $OD_{600}$ = 0.5.
107 IPTG (400 μM) was supplemented for 1 hour to induce ectopic expression of DolP$^{His}$.
108 Cells were visualized on 1% (w/v) agarose pads by fluorescence and phase-contrast
109 microscopy. Bar = 5 μm.

110

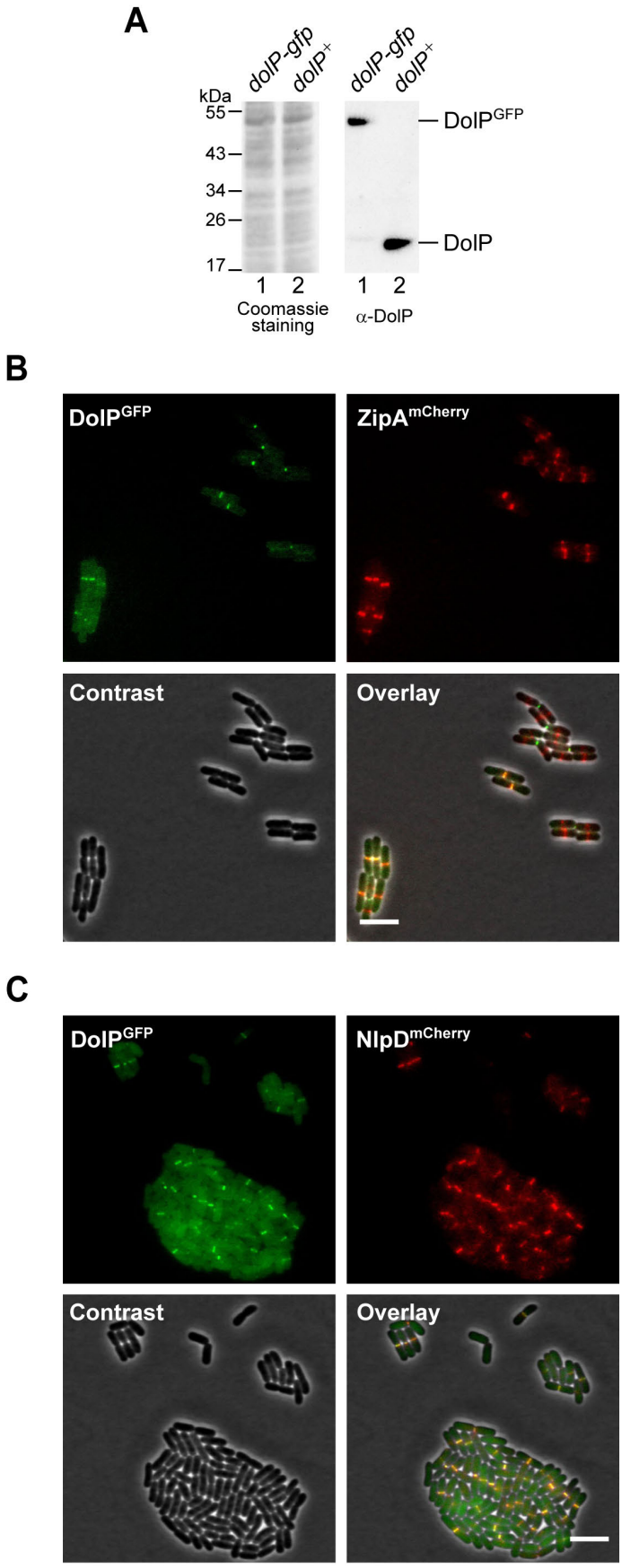


**Figure S6.**

111

112 **Fig. S6. DolP accumulates at mid-cell sites during a late step of cell division.**

113 **(A**) The total protein content of cells harbouring the *dolP-gfp* chromosomal fusion
114 (lanes 1) or wild-type *dolP* (lanes 2) were analyzed by SDS page followed by
115 coomassie staining or immunoblotting using a DolP specific antiserum.

116 (**B,C**) BW25113-derivative cells harbouring the chromosomal fusion *dolP-gfp* and
117 either *zipA-mCherry* (B) or *nlpD-mCherry* (C) were cultured at 30°C in minimal M9
118 medium to $OD_{600}$ = 0.2-0.3 and visualized on 1% (w/v) agarose pads by fluorescence
119 and phase-contrast microscopy. Bar = 5 μm.

120
121

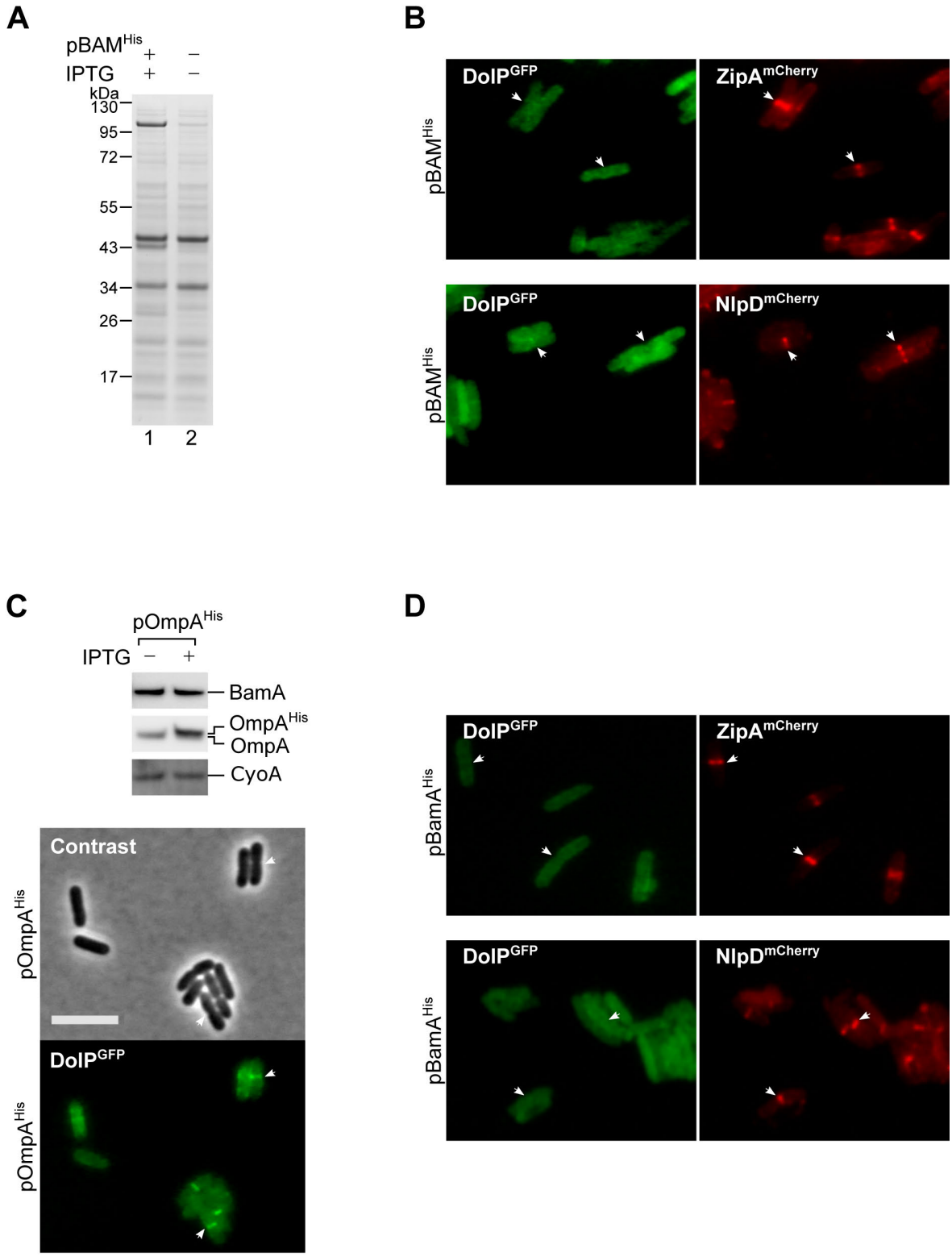
A
pBAM His
IPTG
kDa
130
95
72
55
43
34
26
17
1
2
B
DolP GFP
ZipA mCherry
pBAM His
DolP GFP
NlpD mCherry
pBAM His
C
pOmpA His
IPTG
BamA
OmpA His
OmpA
CyoA
Contrast
pOmpA His
DolP GFP
pOmpA His
D
DolP GFP
ZipA mCherry
pBamA His
DolP GFP
NlpD mCherry
pBamA His

**Figure S7.**

124 **Fig. S7. Overproduction of BAM does not influence septal recruitment of NlpD**
125 **and ZipA.**

126 (**A**) BW25113 cells harbouring pBAM$^{His}$ cultured and supplemented with 400 μM
127 IPTG for 1 hour prior to collecting cells. The protein content of the envelope fraction
128 (lane 1) was analysed by SDS-PAGE and coomassie staining and compared to the
129 protein content of the envelope fraction of BW25113 cells (lane 2).

130 (**B**) BW25113-derivative cells harbouring the chromosomal fusion *dolP-gfp* and *zipA-*
131 *mCherry* or *nlpD-mCherry* were transformed with pBAM$^{His}$ (ectopic overproduction of
132 all BAM subunits, with His-tagged BamE). Cells were then cultured at 30°C in
133 minimal M9 medium supplemented with 400 μM IPTG for 1 hour until $OD_{600}$ = 0.2-
134 0.3, and visualized on 1% (w/v) agarose pads by fluorescence microscopy. The
135 arrowheads indicate the localization of DolP$^{GFP}$, ZipA$^{mCherry}$ or NlpD$^{mCherry}$ at division
136 septa.

137 (**C**) Top: BW25113-derivative *dolP-gfp* cells transformed with pOmpA (ectopic
138 overproduction of His-tagged OmpA) were culture in LB medium and supplemented
139 with 400 mm IPTG or no IPTG for 1 hour prior to collecting cells. The total protein
140 content was analyzed by SDS-PAGE and immunoblotting using the indicated
141 antisera. Bottom: BW25113-derivative *dolP-gfp* cells transformed with pOmpA$^{His}$
142 were cultured in minimal M9 medium supplemented with 400 μM IPTG for 1 hour
143 until $OD_{600}$ = 0.2-0.3, and visualized (B). Bar = 5 μm.

144 (**D**) BW25113-derivative cells harbouring the chromosomal fusion *dolP-gfp* and *zipA-*
145 *mCherry* or *nlpD-mCherry* were transformed with pBamA$^{His}$ (ectopic overproduction
146 of a partially inactive His-tagged form of BamA). Cells were then cultured at 30°C in
147 minimal M9 medium supplemented with 400 μM IPTG for 1 hour until $OD_{600}$ = 0.2-
148 0.3, and visualized as in (B).

149

150
151

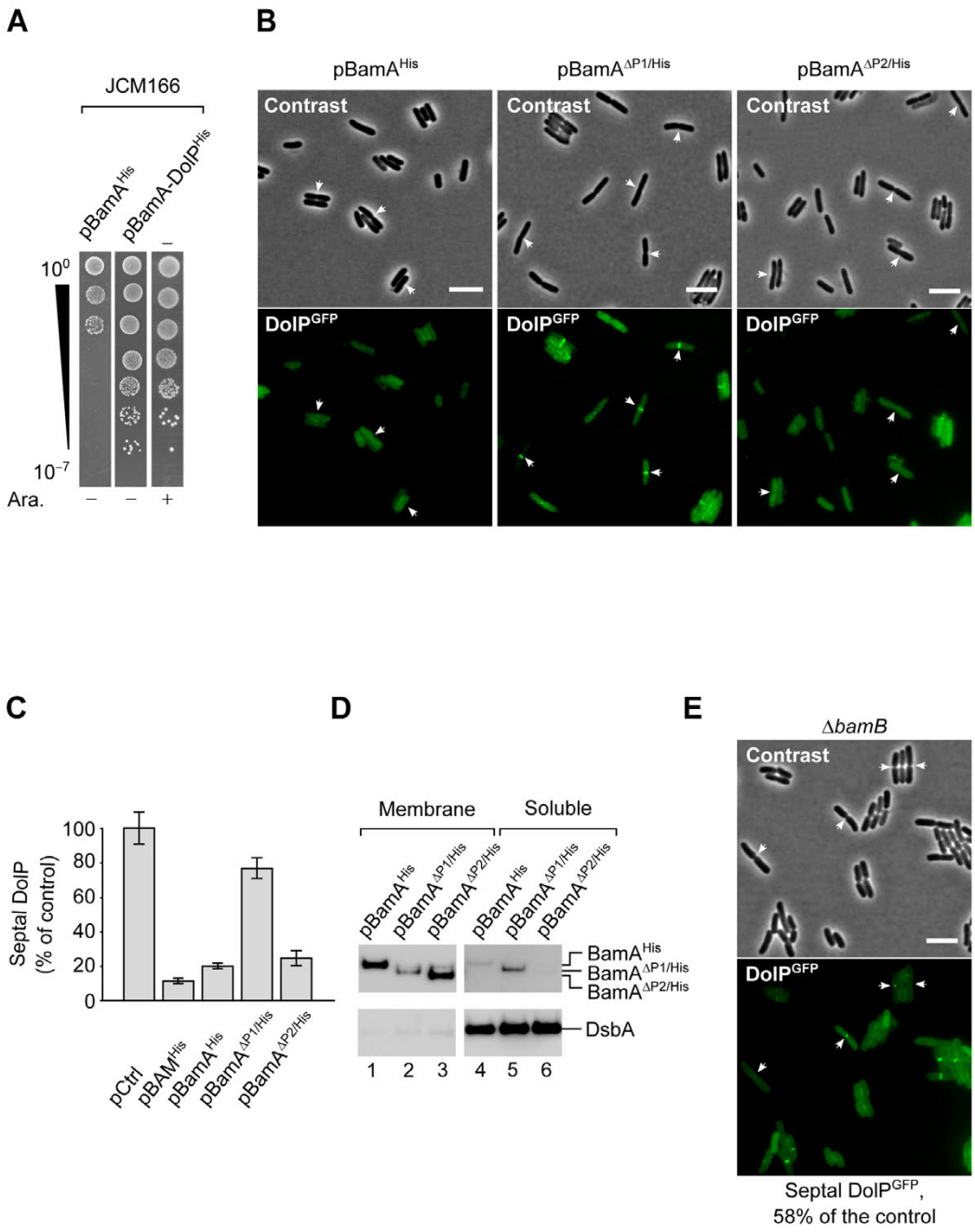
A
JCM166
pBamA^His
pBamA-DolP^His
–
10^0
10^–7
Ara.
– – +
B
pBamA^His
pBamA^ΔP1/His
pBamA^ΔP2/His
Contrast
DolP^GFP
C
Septal DolP (% of control)
100
80
60
40
20
0
pCtrl
pBAM^His
pBamA^His
pBamA^ΔP1/His
pBamA^ΔP2/His
D
Membrane
Soluble
BamA^His
BamA^ΔP1/His
BamA^ΔP2/His
DsbA
1 2 3 4 5 6
E
ΔbamB
Contrast
DolP^GFP
Septal DolP^GFP,
58% of the control

**Figure S8.**

154 **Fig. S8. BamA overaccumulation in the OM and envelope stress impair septal**
155 **DolP localization.**

156 (**A**) The JCM166 BamA depletion strain or its transformants carrying plasmids
157 encoding $BamA^{His}$ or wild-type BamA and DolP were cultured in the presence of
158 0.02% (w/v) arabinose (which induces transcription of a chromosomal copy of wild-
159 type *bamA* engineered downstream of an arabinose-inducible $P_{bad}$ promoter). Serial
160 dilutions were spotted on LB agar devoid of or supplemented with 0.02% (w/v)
161 arabinose, as indicated. In the absence of arabinose, growth is supported by the non-
162 induced, leaky $P_{trc}$ transcription of the wild-type BamA-encoding gene, and not of its
163 variant encoding C-terminally His-tagged BamA.

164 (**B**) Overnight cultures of BW25113 cells harboring the chromosomal *dolP-gfp* fusion
165 and carrying the indicated plasmids were diluted in minimal M9 medium
166 supplemented with 400 μM IPTG. The cells were grown at 30°C to $OD_{600}$ = 0.2-0.3
167 and visualized on 1% (w/v) agarose pads by fluorescence microscopy. The arrows
168 indicate envelope constriction sites between forming daughter cells. Bar = 5 μm.

169 (**C**) Counting of BW25113 cells presenting septal $DolP^{GFP}$ fluorescent signals. *dolP-*
170 *gfp* cells carring $pBAM^{His}$, $pBamA^{His}$, $pBamA^{\Delta P1/His}$ or $pBamA^{\Delta P2/His}$ (analyzed by
171 fluorescence microscopy and shown in Fig. 4A and in Fig. S8B) were counted. The
172 percentage of cells presenting fluorescent $DolP^{GFP}$ signals at the mid-cell in samples
173 overproducing all five BAM subunits or only one of the indicated BamA variants was
174 normalized to the same fraction obtained for cells carrying the control empty vector
175 (pCtrl). Bar charts display a mean value ± SD ($n$ = 3). More than 300 cells were
176 counted in each experiment.

177 (**D**) BW25113 cells carrying the indicated plasmids were cultured and supplemented
178 with 400 μM IPTG to induce ectopic expression of BamA and its mutant forms.
179 Collected cells were subjected to lysozyme/EDTA lysis to obtain the total membrane
180 and soluble fractions. The protein contents of the indicated cell fractions were
181 separated by SDS-PAGE and immunodecorated with the indicated antisera.

182 (**E**) Overnight cultures of Δ*bamB* cells harboring the chromosomal *dolP-gfp* fusion
183 were diluted in minimal M9 medium, cultured at 30°C to $OD_{600}$ = 0.3 and visualized
184 on 1% (w/v) agarose pads by fluorescence microscopy. The arrows indicate
185 envelope constriction sites between forming daughter cells. Bar = 5 μm. The
186 percentage of cells presenting fluorescent $DolP^{GFP}$ signals at division septa in Δ*bamB*
187 cells was normalized to the same fraction obtained for the control cells (BW25113
188 carrying the *dolP-gfp* chromosomal fusion) and reported below the micrograph. More
189 than 300 cells were counted.

190

191

192

193 **Table S1. Log2FC values of sgRNAs in the WT or ΔdolP screen.**

194 See source data file (Table S1)

195

196 **Table S2. Genetic interaction scores.**

197 See source data file (Table S2)

198

199 **Table S3: List of strains**

200

| Name | Genotype and relevant features | Source |
|---|---|---|
| BW25113 | Δ(*araD-araB*)*567* Δ(*rhaD-rhaB*)*568* Δ*lacZ4787*(::*rrnB-3*) *hsdR514 rph-1 (wild-type reference)* | Grenier *et al.*, 2014 [83] |
| Δ*envC* | BW25113 *envC::kan* | This study |
| Δ*rseA* | BW25113 *rseA::kan* | This study |
| Δ*dolP* | BW25113 *dolP::kan* | This study |
| Δ*bamB* | BW25113 *bamB::kan* | This study |
| Δ*bamB* Δ*dolP* | BW25113 Δ*bamB dolP::kan* | |
| Δ*dolP* Δ*rseA* | BW25113 Δ*dolP rseA::kan* | This study |
| *dolP-gfp* | BW25113 *dolP-gfp* | This study |
| Δ*surA dolP-gfp* | BW25113 *surA::kan dolP-gfp* | This study |
| Δ*bamB dolP-gfp* | BW25113 *bamB::kan dolP-gfp* | This study |
| Δ*dolP bamD-mCherry* | BW25113 Δ*dolP bamD-mCherry* | This study |
| *bamD-mCherry* | BW25113 *bamD-mCherry* | This study |
| *dolP-gfp nlpD-mCherry* | BW25113 *dolP-gfp nlpD-mCherry* | This study |
| *dolP-gfp zipA-mCherry* | BW25113 *dolP-gfp zipA-mCherry* | This study |
| JCM166 | MC4100 *ara*$^{r/-}$ Δ(*λatt-lom*)::*bla* $P_{BAD}$*yaeT araC* Δ*yaeT* (BamA depletion strain) | Wu *et al.*, 2005 [84] |
| LC-E75 | $F^-$ $\lambda^-$ *ilvG*$^-$ *rfb-50 rph-1 186attB*::$P_{tet}$-*dcas9*, λ*attB::mCherry* | Cui *et al.*, 2018 [85] |
| LC-E75 Δ*dolP* | LC-E75 *dolP::kan* | This study |

201

202 **Table S4: List of plasmids**

203

| Name | Relevant features | Source |
|---|---|---|
| pCtrl | Reference empty vector for ectopic protein expression | This study |
| pBAM | Ectopic expression of all 5 BAM subunits | This study |
| pBAM$^{His}$ (pJH114) | Ectopic expression of all 5 BAM subunits; BamE is C-terminally His-tagged | Roman Hernandez *et al*., 2014 [86] |
| pBAM$^{ProtA}$ | Ectopic expression of all 5 BAM subunits; BamE is C-terminally Protein A-tagged; a TEV site amino acid linker is positioned immediately upstream of the tag | This study |
| pBAM$^{\Delta P1/ProtA}$ | Ectopic expression of all 5 BAM subunits; BamA harbours the deletion of POTRA1 and BamE is C-terminally Protein A-tagged; a TEV site amino acid linker is positioned immediately upstream of the tag | This study |
| pBAM$^{\Delta P2/ProtA}$ | Ectopic expression of all 5 BAM subunits; BamA harbours the deletion of POTRA2 and BamE is C-terminally Protein A-tagged; a TEV site amino acid linker is positioned immediately upstream of the tag | This study |
| pBamBCDE$^{His}$ | Ectopic expression of BamB, BamC, BamD and BamE subunits; BamE is C-terminally His-tagged | This study |
| pBamA$^{His}$ | Ectopic expression of C-terminally His-tagged BamA | This study |
| pBamA$^{\Delta P1/His}$ | Ectopic expression of a C-terminally His-tagged BamA variant lacking POTRA1 | This study |
| pBamA$^{\Delta P2/His}$ | Ectopic expression of a C-terminally His- | This study |

| | | |
|---|---|---|
| | tagged BamA variant lacking POTRA2 | |
| pBamA-DolP$^{His}$ | Ectopic expression of BamA and C-terminally His-tagged DolP | This study |
| pBamA$^{\Delta P1}$-DolP$^{His}$ | Ectopic expression of a BamA variant lacking POTRA1 and C-terminally His-tagged DolP | This study |
| pBamA$^{\Delta P2}$-DolP$^{His}$ | Ectopic expression of a BamA variant lacking POTRA2 and C-terminally His-tagged DolP | This study |
| pDolP | Ectopic expression of wild-type DolP | This study |
| pDolP$^{ProtA}$ | Ectopic expression of C-terminally protein A-tagged DolP; a TEV site amino acid linker is positioned immediately upstream of the tag | This study |
| pDolP$^{His}$ | Ectopic expression of C-terminally His-tagged DolP | This study |
| pOmpA$^{His}$ | Ectopic expression of C-terminally His-tagged OmpA | This study |
| pRI22 | Ectopic expression of EspP | Ieva *et al.*, 2009 [79] |
| psgRNAcos | Reference empty vector for expression of sgRNAs | Cui *et al.*, 2018 [85] |
| psgRNA*bamD* (pCAT187) | Expression of a *bamD*-specific sgRNA | This study |
| psgRNA*bamE* (pCAT189) | Expression of a *bamE*-specific sgRNA | This study |
| psgRNA*envC* (pCAT191) | Expression of a *envC*-specific sgRNA | This study |
| psgRNA*ftsX* (pCAT193) | Expression of a *ftsX*-specific sgRNA | This study |

204

205

## Supplementary References


78 Ashburner, M., Ball, C. A., Blake, J. A., Botstein, D., Butler, H., Cherry, J. M., Davis, A. P., Dolinski, K., Dwight, S. S., Eppig, J. T., Harris, M. A., Hill, D. P., Issel-Tarver, L., Kasarskis, A., Lewis, S., Matese, J. C., Richardson, J. E., Ringwald, M., Rubin, G. M. & Sherlock, G. Gene ontology: tool for the unification of biology. The Gene Ontology Consortium. *Nature genetics* **25**, 25-29, doi:10.1038/75556 (2000).

79 Ieva, R. & Bernstein, H. D. Interaction of an autotransporter passenger domain with BamA during its translocation across the bacterial outer membrane. *Proceedings of the National Academy of Sciences of the United States of America* **106**, 19120-19125, doi:10.1073/pnas.0907912106 (2009).

80 Albenne, C. & Ieva, R. Job contenders: roles of the beta-barrel assembly machinery and the translocation and assembly module in autotransporter secretion. *Molecular microbiology* **106**, 505-517, doi:10.1111/mmi.13832 (2017).

81 Dautin, N., Barnard, T. J., Anderson, D. E. & Bernstein, H. D. Cleavage of a bacterial autotransporter by an evolutionarily convergent autocatalytic mechanism. *The EMBO journal* **26**, 1942-1952, doi:10.1038/sj.emboj.7601638 (2007).

82 Szabady, R. L., Peterson, J. H., Skillman, K. M. & Bernstein, H. D. An unusual signal peptide facilitates late steps in the biogenesis of a bacterial autotransporter. *Proceedings of the National Academy of Sciences of the United States of America* **102**, 221-226, doi:10.1073/pnas.0406055102 (2005).

83 Grenier, F., Matteau, D., Baby, V. & Rodrigue, S. Complete Genome Sequence of Escherichia coli BW25113. *Genome announcements* **2**, doi:10.1128/genomeA.01038-14 (2014).

84 Wu, T., Malinverni, J., Ruiz, N., Kim, S., Silhavy, T. J. & Kahne, D. Identification of a multicomponent complex required for outer membrane biogenesis in Escherichia coli. *Cell* **121**, 235-245, doi:10.1016/j.cell.2005.02.015 (2005).

85 Cui, L., Vigouroux, A., Rousset, F., Varet, H., Khanna, V. & Bikard, D. A CRISPRi screen in E. coli reveals sequence-specific toxicity of dCas9. *Nature communications* **9**, 1912, doi:10.1038/s41467-018-04209-5 (2018).

86 Roman-Hernandez, G., Peterson, J. H. & Bernstein, H. D. Reconstitution of bacterial autotransporter assembly using purified components. *eLife* **3**, e04234, doi:10.7554/eLife.04234 (2014).